scientific reports

Check for updates

OPEN

In silico design of novel pyridazine derivatives as balanced multifunctional agents against Alzheimer's disease

Mourad Aloui[1✉], Mohamed El fadili[1✉], Somdutt Mujwar[2], Mohammed Er-rajy[1], Hatem A. Abuelizz[3], Sara Er-rahmani[4], Sara Zarougui[1] & Elhalaoui Menana[1]

Alzheimer's disease (AD) necessitates innovative therapeutic approaches that target its multifaceted pathology. This study investigates a series of 2-aminoalkyl-6-(2-hydroxyphenyl)pyridazin-3(2H)-one derivatives as potential multi-target ligands for AD, aiming to simultaneously inhibit acetylcholinesterase (AChE) and amyloid-beta (Aβ) aggregation. To assess the therapeutic potential of these compounds, we employed a comprehensive computational approach, incorporating 2D-QSAR modeling, molecular dynamics simulations, molecular docking, and ADMET property analysis. Based on these analyses, we designed 13 novel pyridazine derivatives exhibiting favorable interactions with key AD-related proteins, enhanced dynamic stability within protein binding sites, and adherence to established drug-likeness principles. Notably, these compounds demonstrated promising oral absorption (96%) and exhibited no significant toxicity in preliminary assessments. These results indicate that the novel pyridazine derivatives warrant further investigation as promising multifunctional agents for the treatment of Alzheimer's disease.

Keywords QSAR, Pyridazine, Molecular docking, Molecular dynamic, ADMET propriety, Alzheimer's disease

Molecular modeling and docking methodologies are increasingly important in drug development, particularly for various diseases such as AIDS, cancer, and Alzheimer's disease (AD)[1–3]. AD is characterized by the appearance of extracellular amyloid-β (Aβ) plaques and intracellular neurofibrillary tangles, neuronal death and the loss of synapses, all of which contribute to progressive cognitive decline. AD is a terminal and incurable disease, with age being the most significant risk factor. It is the most common form of dementia and constitutes ~ 75% of all dementia cases[4]. The prevalence of AD rises exponentially after the age of 65, and the overall prevalence is expected to double within 20 years as average lifespans increase in developing nations[5]. AD is the leading cause of dementia among the elderly, affecting 10% of individuals aged 65 and older, and 50% of those aged 85 and above[6]. According to the World Health Organization, over 55 million people worldwide are living with dementia, with more than 60% residing in low- and middle-income countries[7–9]. The estimated prevalence of dementia among adults aged 60 and above in India is 7.4%, with significant variations observed across different age groups, educational levels, sexes, urban and rural areas and states[10].

The progression of symptoms is associated with changes in the structure of cholinergic synapses in specific brain regions, leading to disruptions in cholinergic neurotransmission[11]. Current drugs for Alzheimer's disease treatment aim to enhance cholinergic neurotransmission by inhibiting the acetylcholinesterase enzyme (AChE), which plays a crucial role in regulating cholinergic neurotransmission by hydrolyzing acetylcholine, a neurotransmitter essential for cognitive function[12]. In the context of Alzheimer's disease, AChE inhibition is a well-established therapeutic strategy for increasing acetylcholine levels in the brain, thereby improving cognitive and memory functions[13]. However, none of the single-target drugs can prevent or reverse the onset or progression of Alzheimer's disease[3,9,14,15]. Furthermore, pyridazin-3(2H)-one is regarded as an enticing structural foundation in drug design, owing to its broad range of bioactivities, notably its anti-inflammatory

[1]LIMAS Laboratory, Faculty of Sciences Dhar El Mahraz, Sidi Mohamed Ben Abdellah University, Fez, Morocco. [2]Chitkara College of Pharmacy, Chitkara University, Rajpura, Punjab 140401, India. [3]Department of Pharmaceutical Chemistry, College of Pharmacy, King Saud University, PO Box 2457, 11451 Riyadh, Saudi Arabia. [4]Dipartimento Di Chimica, Università di Torino, 10125 Torino, Italy. ✉email: mourad.aloui@usmba.ac.ma; mohamed.elfadili@usmba.ac.ma

properties[16–18]. Therefore, the development of novel 2-aminoalkyl-6-(2-hydroxyphenyl)pyridazin-3(2H)-one derivatives as balanced multifunctional agents is preferred for Alzheimer's disease treatment[19]. These derivatives feature a unique chemical structure that combines several important pharmacophoric characteristics[20,21]. The presence of the 2-aminoalkyl group and the pyridazinone core confer high affinity for AChE, while the 2-hydroxyphenyl group enhances solubility and stability[22]. This structural combination not only effectively inhibits AChE but also modulates other biological targets involved in the pathogenesis of Alzheimer's disease, such as beta-amyloid aggregates and oxidative stress[23,24]. Therefore, the development of novel 2-aminoalkyl-6-(2-hydroxyphenyl) pyridazin-3(2H)-one derivatives as balanced multifunctional agents is preferred for Alzheimer's disease treatment[25]. In recent years, researchers have effectively used this structural framework to create cholinesterase inhibitors (ChEIs)[26]. In vitro biological tests showed that most of the hybrid compounds had strong inhibitory activity against AChE, excellent antioxidant properties, and a moderate ability to inhibit $A\beta_{1-42}$ aggregation[14].

To investigate the biological inhibitory activity of forty-six novel small molecules derived from 2-aminoalkyl-6-(2-hydroxyphenyl)pyridazin-3(2H)-one as novel balanced multifunctional agents against Alzheimer's disease, we conducted an in silico study using various molecular modeling techniques[27], namely density functional theory (DFT), 2D-QSAR, molecular docking, drug-like ADMET and pharmacokinetic properties analysis[28]. Finally, 100 ns molecular dynamics (MD) simulations were performed to estimate the stability of the ligand-receptor complex under normal physiological conditions[29–31]. Our research utilized a comprehensive approach that included 2D-QSAR modeling, molecular dynamics simulations, molecular docking, and ADMET property analysis. The aim was to investigate and design new pyridazin-derived small molecules that demonstrate strong inhibition as innovative balanced multifunctional candidates for Alzheimer's disease treatment, while optimizing pharmacokinetic properties and enhancing structural stability. By integrating these methodologies, the study sought to understand the structural and dynamic properties of these compounds, their interactions with biological targets, and their pharmacokinetic and safety profiles. This multi-faceted evaluation provides a robust framework for identifying and developing effective therapeutic candidates for Alzheimer's disease. This project is divided into two chapters: the first describes the materials and methods used in this research, followed by another chapter devoted to a detailed discussion of the results obtained from computer simulations, and the final section summarizes the main findings and overall implications of this research.

Materials and methods

Experimental dataset

The experimental biological activities regarding forty-six 2-aminoalkyl-6-(2-hydroxyphenyl)pyridazin- 3(2H)-one derivatives as balanced multifunctional agents against Alzheimer's disease are provided in Table 1, in which the 2D structures were drawn using Chem-Draw software.

Examined compounds

For the purpose of molecular modeling, we employed empirical data regarding the inhibitory effects of the 46 pyridazine-based compounds. These compounds had been earlier synthesized with a focus on balanced multifunctionality against Alzheimer's disease[14]. The recorded inhibitory activities (IC_{50}) were subsequently converted into (pIC_{50}) values using a logarithmic transformation of the IC_{50} scale. The resulting data is outlined The experimental biological activities regarding forty-six 2-aminoalkyl-6-(2-hydroxyphenyl)pyridazin- 3(2H)-one derivatives as balanced multifunctional agents against Alzheimer's disease are provided in Table 1.

Calculation of descriptors for the compounds studied

To construct a reliable QSAR model, a comprehensive set of 31 descriptors was employed. These descriptors included various factors such as lipophilicity, geometric attributes, physicochemical properties and steric characteristics. Molecular descriptors were calculated using the MM2 technique with ACD/ChemSketch[32] and ChemBioOffice software[33]. To optimize molecular geometry, density functional theory (DFT) calculations were performed using the 6-31G basis set and B3LYP functional[34,35]. Electronic descriptors were also calculated using Gaussian 03 quantum chemistry software[36]. The calculated descriptor values are summarized in Table 2.
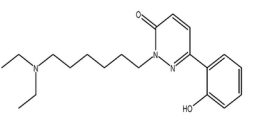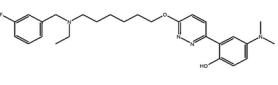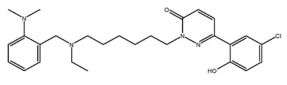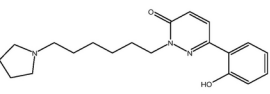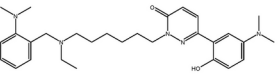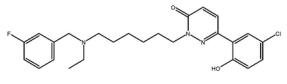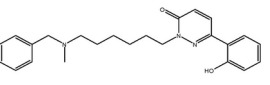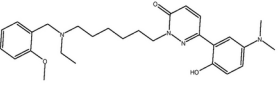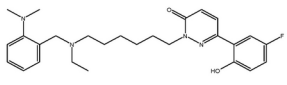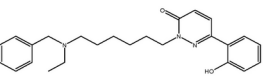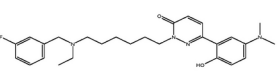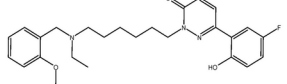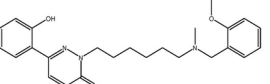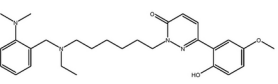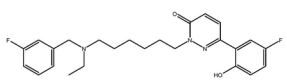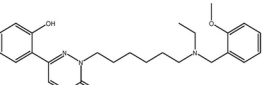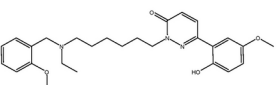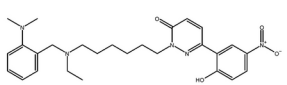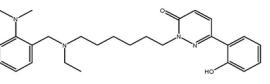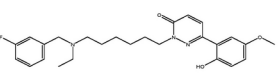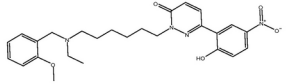
Quantitative structure–activity relationship modeling

To develop a QSAR model, a set of 46 molecules was chosen from prior research based on their substantial activity as balanced multifunctional agents against Alzheimer's disease. This set was randomly partitioned into two subsets: a training set consisting of 37 molecules to construct the model, and a test set consisting of 9 molecules to evaluate the model's validity. Several statistical techniques, including multiple linear regression (MLR) and artificial neural networks (ANN), were utilized to establish the QSAR model[37].

Multiple linear regression

Multiple linear regression (MLR) is a commonly used method in QSAR studies due to its simplicity and reliability in identifying relevant molecular descriptors[38]. To enhance the QSAR model's predictive power, we combined MLR with multiple nonlinear regression (MNLR) and ANN methods. This integrated approach allowed us to identify the most relevant molecular descriptors for use in model development. The basic assumption of MLR is that the dependent variable has a linear relationship with specific independent variables, as illustrated by the following equation:

$$Y = a_0 + \sum_{i=1}^{n} a_i X_i \tag{1}$$

Comp	Structure	pIC$_{50}$	Comp	Structure	pIC$_{50}$	Comp	Structure	pIC$_{50}$
1		5.61	17		4.31	33*		6.13
2		5.80	18		6.70	34		5.84
3		6.03	19		5.92	35		6.80
4		6.04	20		6.46	36		6.24
5		5.97	21		6.48	37		6.60
6		6.13	22		6.20	38		6.34
7		6.21	23*		5.64	39		5.94

Table 1. Structures and pIC$_{50}$ values of novel 2-aminoalkyl-6-(2-hydroxyphenyl)pyridazin- 3(2H)-one. *Indicate the test set compounds, pIC$_{50}$ = 6-log$_{10}$ (IC$_{50}$).
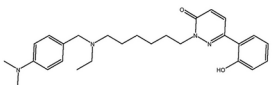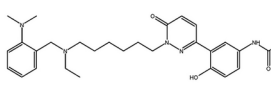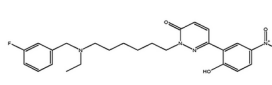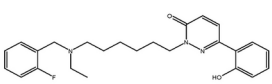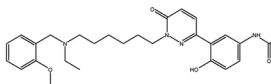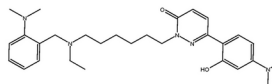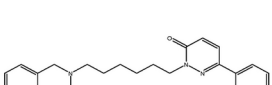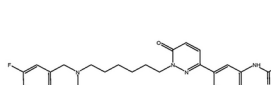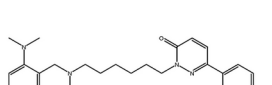
8		5.04	24		7.07	40		6.00
9		5.99	25		6.43	41		5.67
10		6.17	26		7.16	42		5.80
11		5.07	27		6.55	43		5.93
12*		5.64	28		5.78	44*		4.78
13		5.53	29*		6.05	45*		5.57

Table 1. (continued)

where Y denotes the dependent variable, X_i signify the independent variables, n represents the number of molecular descriptors, a_0 corresponds to the constant component of Eq. (1), and a_i denote the coefficients of the molecular descriptors.

MLR-QSAR modeling efficiency

Multiple nonlinear regression

Identifying a predictive model that accurately reflects the non-linear interactions between biological activity (Y) and calculated molecular descriptors (X_i) is crucial in quantitative structure–activity relationship (QSAR) studies. While several non-linear regression methods exist[39], this investigation utilized a second-order polynomial regression to construct the QSAR model. This approach aims to capture the quadratic relationships that may exist between the descriptors and predicted activity. The model is represented by the following equation:

Table 1. (continued)

$$Y = a_0 + \sum_{i=1}^{n} a_i \times X_i + b_i \times X_i^2 \qquad (2)$$

This equation diverges from traditional multiple linear regression by incorporating squared terms, allowing for the modeling of curvilinear relationships. In this context, 'Y' signifies the predicted biological activity, while 'X_i' represents the molecular descriptors, with 'n' denoting the total number of descriptors included in the model. The coefficients 'a_o', 'a_i', and 'b_i' represent, respectively, the intercept, the linear coefficients associated with each descriptor, and the quadratic coefficients that quantify the influence of the squared descriptor terms. This formulation enables a more nuanced understanding of how variations in molecular features translate into changes in biological activity, particularly when non-linear dependencies are prevalent.

Leave one out cross-validation
To evaluate the precision of the QSAR models generated using MLR, MNLR, and ANN techniques, we employ an internal validation approach referred to as LOO-CV[40]. To assess the model's robustness, we conducted leave-one-out cross-validation (LOO-CV). In this process, each molecule was sequentially removed from the dataset, and the remaining molecules were used to train a QSAR model to predict the activity of the excluded molecule[28]. This procedure was repeated for all molecules in the dataset[38]. This validation approach relies on calculating the R_{cv}^2 coefficient of performance, as described in Eq. (3). Following this methodology, we can assess the model's accuracy and determine its predictive capabilities[40], Ideally, the R_{cv}^2 value should exceed 0.5, indicating that the developed model demonstrates robustness concerning internal predictions.

$$R_{cv}^2 = 1 - \frac{\sum \left(Y_{ob}\left(trai\right) - Y_{ca}\left(trai\right)\right)^2}{\sum \left(Y_{Ob}\left(trai\right) - \overline{Y_{trai}}\left(trai\right)\right)^2} \qquad (3)$$

$Y_{ob}\left(train\right)$ refers to the actual observed response value in the training set. $Y_{ca}\left(trai\right)$ represents the response value predicted by the LOO-CV technique applied to the training set. Lastly, $\overline{Y_{trai}}(trai)$ denotes the mean value of both the observed and predicted responses in the training set.

Artificial neural networks
To enhance the prediction of biological activity, we developed an ANN-based QSAR model using the molecular descriptors derived from the MLR model. The ANN model aims to establish a more accurate relationship between these descriptors and the observed biological activity levels[41]. This approach employs a sigmoid activation function in the hidden layer and a linear activation function in the output layer[37]. The ANN design employed in this work is made up of three neuron layers: the input layer, the hidden layer, and the output layer, as seen in Fig. 1.

The first layer of the neural network has several neurons equal to or less than the total number of descriptors used in the multiple linear regression model. The output layer represents the predicted activity levels. A key

Comp	S	B	S-B	Tor	1.4 VDW	LogP	W	NHBA	NHBD	BI	MTI	NRB	PSA	SOV	SOVD	TD
1	2.74	9.10	0.57	−1.05	22.60	3.201	343.471	4	1	787,896	13,895	10	56.14	52	78	15
2	2.46	9.52	0.22	3.88	22.03	2.84	341.455	4	1	612,230	13,863	8	56.14	54	80	15
3	2.65	7.67	0.42	−10.09	26.86	4.257	391.515	4	1	1,291,975	22,084	10	56.14	62	94	18
4	2.79	8.92	0.53	−9.14	27.33	4.595	405.542	4	1	1,495,116	23,949	11	56.14	64	96	18
5	3.13	10.25	0.44	−11.12	29.71	4.131	421.541	5	1	1,760,073	25,923	11	65.37	66	102	18
6	3.32	9.80	0.48	−5.69	30.90	4.469	435.568	5	1	2,009,533	27,880	12	65.37	68	104	18
7	4.79	19.22	0.98	−8.34	31.69	4.88	448.611	5	1	2,310,469	30,536	12	59.38	70	104	18
8	3.39	13.58	0.83	−10.53	31.32	4.88	448.611	5	1	2,390,269	31,598	12	59.38	70	104	20
9	2.91	8.65	0.50	−8.52	27.82	4.754	423.532	5	1	1,733,763	25,244	11	56.14	66	104	18
10	2.86	8.55	0.50	−8.48	27.70	4.754	423.532	5	1	1,745,538	25,357	11	56.14	66	104	18
11	2.86	8.53	0.50	−8.46	27.70	4.754	423.532	5	1	1,757,103	25,470	11	56.14	66	104	19
12*	3.08	9.13	0.53	−8.34	28.43	5.154	439.984	4	1	1,733,763	25,244	11	56.14	66	98	18
13	2.88	8.55	0.51	−8.44	28.29	5.154	439.984	4	1	1,745,538	25,357	11	56.14	66	98	18
14*	3.21	9.12	0.51	−9.49	28.55	5.082	419.569	4	1	1,733,763	26,072	11	56.14	66	98	18
15	2.73	7.92	0.40	−10.28	28.71	4.236	403.526	4	1	1,224,678	23,765	8	56.14	66	98	18
16	5.70	29.87	1.57	−12.81	36.89	6.636	491.68	7	1	3,756,429	41,881	14	63.9	76	112	21
17	3.71	18.14	1.00	−12.12	33.02	6.51	466.601	7	1	2,905,136	35,330	13	60.66	72	112	21
18	5.40	24.15	1.33	−10.90	35.01	5.165	491.68	6	1	3,446,699	38,396	13	62.62	76	112	19
19	4.05	16.31	0.89	−12.47	33.94	4.754	478.637	6	1	3,027,704	35,257	13	68.61	74	112	19
20	3.49	13.65	0.87	−11.25	31.02	5.038	466.601	6	1	2,656,839	32,265	12	59.38	72	112	19
21	5.13	21.81	1.06	−8.85	34.10	4.754	478.637	6	1	3,030,515	35,240	13	68.61	74	112	19
22	3.79	13.99	0.62	−10.44	33.03	4.343	465.594	6	1	2,653,856	32,289	13	74.6	72	112	19
23*	3.22	11.32	0.59	−9.20	30.11	4.627	453.558	6	1	2,321,395	29,479	12	65.37	70	112	19
24	4.87	22.35	0.97	−9.05	31.65	3.788	505.663	6	2	3,941,426	40,955	14	88.48	78	120	20
25	3.52	14.54	0.53	−10.64	30.57	3.377	492.62	6	2	3,473,954	37,668	14	94.47	76	120	20
26	2.95	11.87	0.50	−9.41	27.66	3.661	480.584	6	2	3,058,919	34,531	13	85.24	74	120	20
27	4.84	19.44	0.98	−9.66	32.25	5.367	462.638	5	1	2,646,445	33,085	12	59.38	72	106	18
28	3.49	11.61	0.54	−11.24	31.18	4.956	449.595	5	1	2,309,611	30,268	12	65.37	70	106	18
29*	2.93	8.94	0.51	−10.00	28.25	5.241	437.559	5	1	2,013,217	27,589	11	56.14	68	106	18
30*	4.86	19.27	1.00	−8.93	32.45	5.709	527.507	5	1	2,646,445	32,104	12	59.38	72	106	18
31	3.51	11.45	0.56	−10.51	31.38	5.298	514.464	5	1	2,309,611	29,341	12	65.37	70	106	18
32	2.95	8.77	0.53	−9.26	28.46	5.582	502.428	5	1	2,013,217	26,713	11	56.14	68	106	18
33*	4.85	19.25	0.98	−8.93	32.27	5.438	483.053	5	1	2,646,445	32,104	12	59.38	72	106	18
34	2.93	8.74	0.51	−9.27	28.28	5.312	457.974	5	1	2,013,217	26,713	11	56.14	68	106	18
35	4.80	19.31	0.97	−8.96	31.56	5.038	466.601	6	1	2,646,445	32,104	12	59.38	72	112	18
36	3.45	11.49	0.53	−10.55	30.47	4.627	453.558	6	1	2,309,611	29,341	12	65.37	70	112	18
37	2.89	8.81	0.50	−9.31	27.56	4.912	441.523	6	1	2,013,217	26,713	11	56.14	68	112	18
38	4.94	20.07	1.00	−8.37	33.86	5.811	493.608	6	1	3,446,699	36,912	13	111.19	76	112	19
39	3.60	12.24	0.56	−9.92	32.77	5.108	480.565	6	1	3,027,704	33,850	13	117.18	74	122	19
40	3.05	9.57	0.53	−8.65	29.85	5.113	468.529	6	1	2,656,839	30,931	12	107.95	72	122	19
41	5.07	24.48	1.28	−11.11	35.23	5.165	491.68	6	1	3,495,908	38,959	13	62.62	76	112	20
42	4.93	21.81	1.04	−8.98	34.36	4.754	478.637	6	1	3,061,390	35,582	13	68.61	74	112	20
43	4.79	19.29	0.97	−8.97	31.56	5.038	466.601	6	1	2,661,023	32,225	12	59.38	72	112	19
44*	5.54	24.30	1.38	−10.86	36.37	6	519.734	6	1	4,694,352	47,137	15	62.62	80	116	21
45*	5.01	22.55	1.01	−9.06	33.02	4.623	533.717	6	2	5,323,809	50,050	16	88.48	82	124	22
46*	5.64	28.85	1.47	−12.04	37.00	6.636	491.68	7	1	3,756,429	41,881	14	63.9	76	112	21

Comp	TC	TVC	FW	MR	MV	Par	IR	ST	D	Polar	E_{HOMO}	E_{LUMO}	E_T	Dp	repul	pIC_{50}
1	0.0002	2.36E-06	343.463	101.92	316.5	801.2	1.557	41	1.08	4E-23	−0.1933	−0.077	−1094	2.47	2004.27	5.61
2	0.0001	1.18E-06	341.447	99.74	289.8	761.5	1.604	47.6	1.17	4E-23	−0.1955	−0.077	−1092.8	2.84	1983.93	5.80
3	2.95E-05	1.07E-07	391.506	117.99	353.1	908.4	1.582	43.7	1.1	4.7E-23	−0.2015	−0.0777	−1246.4	2.46	2384.42	6.03
4	2.09E-05	7.58E-08	405.533	122.6	369.2	947	1.578	43.2	1.09	4.9E-23	−0.1953	−0.0776	−1285.7	2.40	2534.73	6.04
5	1.71E-05	3.79E-08	421.532	123.8	374.8	958.6	1.574	42.7	1.12	4.9E-23	−0.1887	−0.0764	−1360.8	2.34	2723.82	5.97
6	1.21E-05	2.68E-08	435.559	128.41	390.8	997.3	1.57	42.3	1.11	5.1E-23	−0.1949	−0.0763	−1400.1	3.53	2882.32	6.13
7	9.84E-06	2.93E-08	448.6	135.4	410.3	1043.3	1.574	41.7	1.09	5.4E-23	−0.1905	−0.0772	−1419.6	3.41	3030.17	6.21
8	9.84E-06	2.93E-08	448.6	135.4	410.3	1043.3	1.574	41.7	1.09	5.4E-23	−0.174	−0.0764	−1419.6	2.78	2968.55	5.04
9	1.71E-05	2.48E-08	423.523	122.47	372	947.2	1.572	41.9	1.13	4.9E-23	−0.2044	−0.0774	−1384.9	0.95	2727.71	5.99
Continued																

| Comp	TC	TVC	FW	MR	MV	Par	IR	ST	D	Polar	E_{HOMO}	E_{LUMO}	E_T	Dp	repul	pIC_{50}
10	1.71E-05	2.48E-08	423.523	122.47	372	947.2	1.572	41.9	1.13	4.9E-23	−0.2065	−0.0785	−1384.9	2.51	2690.49	6.17
11	1.71E-05	2.48E-08	423.523	122.47	372	947.2	1.572	41.9	1.13	4.9E-23	−0.2066	−0.0786	−1384.9	3.84	2687.10	5.07
12*	1.71E-05	7.44E-08	439.978	127.2	378.5	975.8	1.586	44.1	1.16	5E-23	−0.2063	−0.0776	−1745.2	0.69	2858.12	5.64
13	1.71E-05	7.44E-08	439.978	127.2	378.5	975.8	1.586	44.1	1.16	5E-23	−0.2087	−0.0789	−1745.2	2.83	2800.37	5.53
14*	1.71E-05	6.56E-08	419.559	127.02	384.4	978.1	1.574	41.9	1.09	5E-23	−0.1994	−0.077	−1325	2.85	2725.56	5.60
15	1.21E-05	4.64E-08	403.517	120.23	341.5	899.7	1.621	48.1	1.18	4.8E-23	−0.2013	−0.0758	−1284.5	2.56	2514.70	5.59
16	4.02E-06	1.14E-08	491.668	149.48	439.5	1160.7	1.595	48.6	1.118	5.9E-23	−0.169	−0.0623	−1553.5	8.08	3385.17	5.37
17	6.96E-06	9.61E-09	466.591	135.16	405.8	1065.8	1.58	47.5	1.149	5.4E-23	−0.1687	−0.0621	−1518.8	6.89	3044.40	4.31
18	4.64E-06	1.14E-08	491.668	148.21	451.4	1139.6	1.57	40.6	1.08	5.9E-23	−0.1824	−0.0697	−1553.5	4.53	3462.97	6.70
19	5.68E-06	1.04E-08	478.626	141.22	431.9	1093.6	1.567	41	1.1	5.6E-23	−0.1819	−0.069	−1534.1	3.84	3320.36	5.92
20	8.04E-06	9.61E-09	466.591	135.27	413.1	1043.5	1.568	40.6	1.12	5.4E-23	−0.1838	−0.0713	−1518.8	5.91	3121.46	6.46
21	5.68E-06	1.04E-08	478.626	141.22	431.9	1093.6	1.567	41	1.1	5.6E-23	−0.19	−0.077	−1534.1	2.32	3304.41	6.48
22	6.96E-06	9.47E-09	465.585	134.23	412.4	1047.5	1.564	41.5	1.12	5.3E-23	−0.1954	−0.0763	−1514.6	1.93	3163.15	6.20
23*	9.84E-06	8.77E-09	453.549	128.28	393.7	997.4	1.565	41.1	1.15	5.1E-23	−0.2072	−0.0786	−1499.4	3.22	2966.81	5.64
24	3.28E-06	2.59E-09	505.652	148.34	443.4	1138.4	1.583	43.4	1.14	5.9E-23	−0.1907	−0.0797	−1627.5	2.86	3553.58	7.07
25	4.02E-06	2.37E-09	492.61	141.35	423.9	1092.4	1.581	44	1.16	5.6E-23	−0.1959	−0.0787	−1608.1	2.99	3409.90	6.43
26	5.68E-06	2.19E-09	480.574	135.41	405.2	1042.3	1.582	43.7	1.18	5.4E-23	−0.208	−0.0815	−1592.8	2.57	3210.56	7.16
27	8.04E-06	2.54E-08	462.627	139.83	425.5	1074.4	1.571	40.6	1.08	5.5E-23	−0.1894	−0.0757	−1458.9	2.83	3138.27	6.55
28	9.84E-06	2.32E-08	449.585	132.84	406	1028.3	1.568	41.1	1.1	5.3E-23	−0.1951	−0.075	−1439.5	2.68	3000.41	5.78
29*	1.39E-05	2.15E-08	437.55	126.89	387.2	978.3	1.569	40.7	1.12	5E-23	−0.2066	−0.0774	−1424.2	4.45	2804.83	6.05
30*	8.04E-06	2.54E-08	527.496	142.96	422.8	1086.9	1.591	43.6	1.24	5.7E-23	−0.1901	−0.0838	−3990.6	2.71	3568.06	6.60
31	9.84E-06	2.32E-08	514.455	135.97	403.3	1040.8	1.589	44.3	1.27	5.4E-23	−0.1954	−0.0831	−3971.1	2.73	3424.45	6.06
32	1.39E-05	2.15E-08	502.419	130.03	384.6	990.7	1.591	44	1.3	5.2E-23	−0.2072	−0.0856	−3955.8	3.37	3221.45	5.59
33*	8.04E-06	2.88E-08	483.045	140	419.6	1072.2	1.581	42.6	1.15	5.6E-23	−0.1903	−0.0849	−1879.2	2.95	3265.02	6.13
34	1.39E-05	2.44E-08	457.968	127.07	381.3	976	1.58	42.9	1.2	5E-23	−0.2073	−0.0866	−1844.5	3.39	2928.61	5.84
35	8.04E-06	9.61E-09	466.591	135.27	413.1	1043.5	1.568	40.6	1.12	5.4E-23	−0.1899	−0.083	−1518.8	2.79	3141.35	6.80
36	9.84E-06	8.77E-09	453.549	128.28	393.7	997.4	1.565	41.1	1.15	5.1E-23	−0.1958	−0.0825	−1499.4	2.80	3002.26	6.24
37	1.39E-05	8.12E-09	441.513	122.34	374.9	947.3	1.566	40.7	1.17	4.9E-23	−0.2073	−0.847	−1484.1	3.43	2806.77	6.60
38	4.64E-06	1.89E-09	493.598	141.06	415.5	1088.8	1.594	47.1	1.18	5.6E-23	−0.1908	−0.1051	−1624	5.37	3426.04	6.34
39	5.68E-06	1.73E-09	480.556	134.07	396	1042.7	1.592	48	1.21	5.3E-23	−0.197	−0.1047	−1604.6	5.64	3285.21	5.94
40	8.04E-06	1.60E-09	468.521	128.13	377.3	992.6	1.594	47.9	1.24	5.1E-23	−0.2082	−0.1064	−1589.3	4.77	3085.53	6.00
41	4.64E-06	1.14E-08	491.668	148.21	451.4	1139.6	1.57	40.6	1.08	5.9E-23	−0.2073	−0.0866	−1844.5	3.39	2928.61	5.67
42	5.68E-06	1.04E-08	478.626	141.22	431.9	1093.6	1.567	41	1.1	5.6E-23	−0.1889	−0.0742	−1534.1	3.90	3275.47	5.80
43	8.04E-06	9.61E-09	466.591	135.27	413.1	1043.5	1.568	40.6	1.12	5.4E-23	−0.1903	−0.0826	−1518.8	1.63	3131.68	5.93
44*	2.32E-06	5.68E-09	519.721	157.43	483.4	1216.8	1.564	40.1	1.07	6.2E-23	−0.1823	−0.0695	−1632.1	4.20	3674.58	4.78
45*	1.64E-06	1.30E-09	533.705	157.56	475.4	1215.7	1.576	42.7	1.12	6.2E-23	−0.1985	−0.0882	−1706.5	2.76	3772.45	5.57
46*	4.02E-06	1.14E-08	491.668	149.48	439.5	1160.7	1.595	48.6	1.118	5.9E-23	−0.1686	−0.0618	−1553.5	7.81	3369.37	5.66

Table 2. Descriptor results calculated for the 46 compounds and observed activity. B, Bend energy (kcal/mol); T, Torsion energy (kcal/mol); Mw, Molecular weight (g/mol); WI, Wiener Index; MV, Molar Volume (cm³); ST, Surface Tension (dyne/cm); D, Density (g/cm³); E_{HOMO}, Energy of the Highest occupied molecular orbital (Hartree); S, Stretch energy (kcal/mol); S-B, Stretch-Bend energy (kcal/mol); NHBA, number of hydrogen bond acceptors; PSA, Polar Surface Area; MR, Molar Refractivity index; IR, Index of Refraction; E_T, total energy (Hartree); repul, repulsion energy (Hartree); E_{LUMO}, Energy of the lowest unoccupied molecular orbital (Hartree). *Indicate the test set compounds.

parameter in the neural network is ρ, which determines the learning rate. To ensure a robust and reliable model, ρ should ideally be between 1 and 3[42].

Y-randomization test
To evaluate the model's robustness and mitigate the potential effects of random correlations, we conducted Y-randomization testing. In this process, the observed biological activity values were randomly shuffled while keeping the molecular descriptors fixed[28]. By generating multiple models with these randomized datasets, we assessed the model's performance against random chance[43]. A QSAR model is considered acceptable if the average random correlation coefficient (R_r^2) from the randomized models is lower than the original model's correlation coefficient (R^2), indicating that the model's performance exceeds what could be attributed to random associations[38].
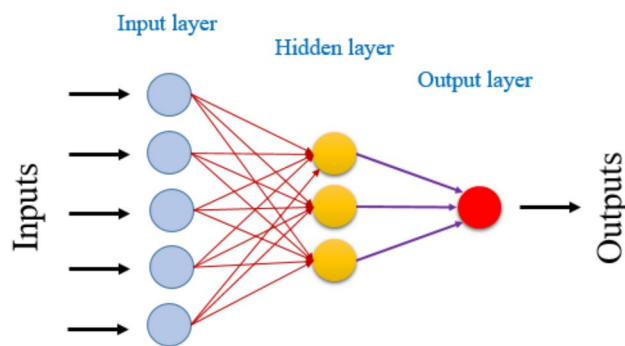
Fig. 1. The architecture of the ANN model used in this study.

Applicability domain
The applicability domain step is employed to explore the predictive power of the developed QSAR model and find the outliers among the training and test sets. To get the applicability domain, the diagonal Hat Matrix (H), which is a projection matrix, must be calculated[28]. The hat matrix is also known as the projection matrix, and its elements are known as the advantage (h_i). The hat matrix (7373) has been calculated by projecting the observations (Y) on predicted values $(\widehat{Y})$ using the following equation:

$$h_i = x_i \left(X^T X \right)^{-1} x_i^T \ i = 1, 2, \ldots, n \tag{4}$$

where x_i is the row vector of descriptors for every compound studied, X is the matrix of descriptors in the training set, and T is the transpose of the defined vector or matrix. The elements of the hat matrix are known as the leverage (h_i), which shows the effect of a particular observation on the predicted values relative to its position in the chemical space of all of the inputs[44]. The leverage values were used to get the applicability domain and the detection of any aberrant compounds in the data set. To this end, the values of the normalized residuals of both the training and test runs have been represented in terms of the leverage values taken from the corresponding hat matrix.

Molecular docking simulations
In the present work, three candidate ligands labelled C25, C27 and Pred12 have been selected to undergo molecular docking processes in order make discoveries about the inhibitory mechanisms of novel 2-aminoalkyl-6-(2-hydroxyphenyl)pyridazin-3(2H)-one derivatives as balanced multifunctional agents against Alzheimer's disease towards the three-dimensional structure of the anti-alzheimer drug complexed with its target acetylcholinesterase (https://www.rcsb.org/structure/1EVE).

Initially, the protein target coded 1EVE.pdb was prepared to meet the standard protocol by removing all suspended ligands bound to protein, including water molecules and acetylcholinesterase co-crystallized ligand, followed by adding Gasteiger charges[45–47]. Subsequently, the prepared protein was converted from PDB to PDBQT form with the assistance of Autodock software, then the candidate ligands were docked to the prepared protein. Finally, Discovery Studio software was used to explore the produced intermolecular interactions in two and three dimensions[48–51].

Molecular dynamics
Ligands 61, 726, and 794 were selected for molecular dynamics (MD) simulations based on their docking scores and observed interactions with acetylcholinesterase (AChE). MD simulations were performed on the AChE complexes with these ligands for 100 ns using the Desmond module in Schrödinger's Maestro software[52–57]. Explicit solvent molecules were added and neutralized with appropriate ions. The system was initially relaxed using the steepest-descent algorithm to minimize energy and eliminate steric clashes. To equilibrate the system, a short series of constant pressure (NPT) simulations with gradually increasing temperature and positional constraints were applied[58]. This ensures a stable, balanced state before the main 100 ns production run, which captures system energies, atom positions, and RMSD values to understand the complex's dynamic behavior and long-term stability[59–64].

In silico pharmacokinetic-pharmacodynamic modeling (ADMET)
Advancements in computer technology have significantly accelerated drug discovery by reducing the need for extensive experimental investigations. Early-stage identification of ADMET pharmacokinetic characteristics and drug similarity has become a standard practice. In silico studies evaluate critical ADMET parameters, including absorption, distribution, metabolism, excretion, and toxicity, which are essential for drug development[65]. To predict drug-likeness, the Lipinski, Ghose, Veber, Egan, and Muegge criteria are used. Lipinski, Veber, and Egan's rules are particularly useful for assessing ADME properties of human drugs based on the 2D structure of small molecules and their oral bioavailability[66]. Compounds that violate two or more of these rules often face ADMET-related challenges. Approximately 10% of drugs in the clinical trial phase do not adhere to any of these
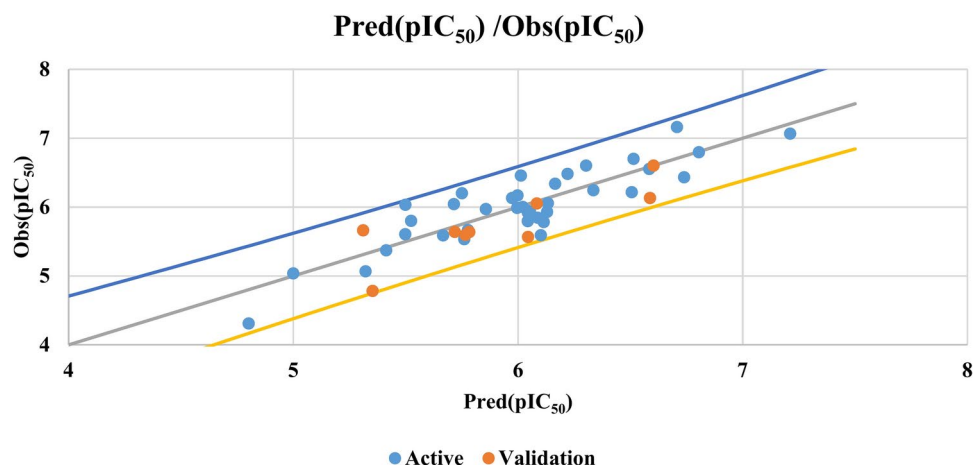
Pred(pIC$_{50}$) /Obs(pIC$_{50}$)

Fig. 2. Comparison of predicted and observed activity values using the MLR model.

pIC$_{50}$ / Normalized coefficients (confidence interval of 95%)
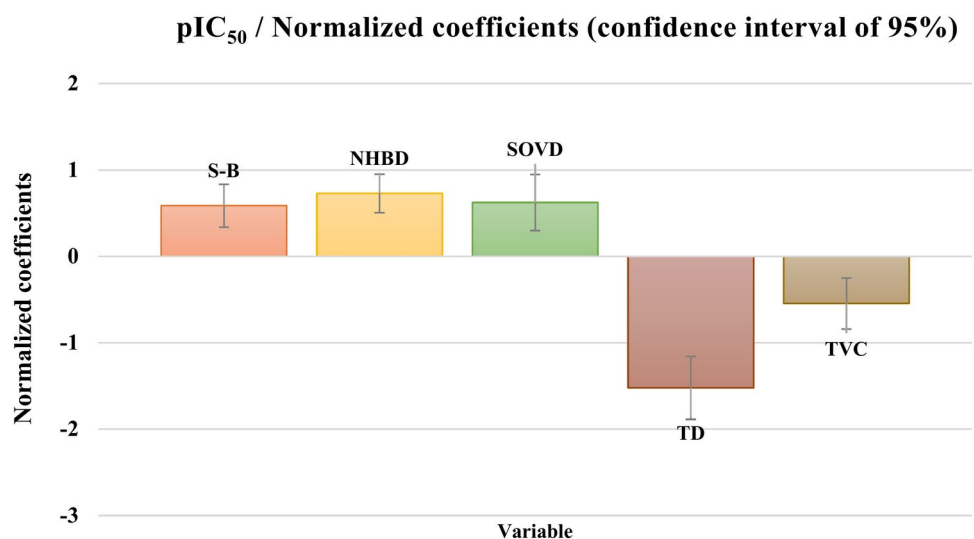

Fig. 3. Analysis of molecular descriptor contributions in an MLR model.

rules. To further understand molecule-receptor interactions, the number of rotational bonds (n-ROTB) and topological polar surface area (TPSA) are also assessed[67].

Results and discussion
Multiple linear regression
After calculating molecular descriptors for 46 derivatives (Table 2), a reliable model was built using five descriptors: S-B, NHBD, SOVD, TD, and TVC. Molecules 12, 14, 23, 29, 30, 33, 44, 45, and 46 were chosen for the test set, while the remaining molecules were included in the training set. The QSAR model produced by the MLR technique is shown in Eq. (5)

$$\mathbf{pIC}_{50} = 12.46558 + 1.07186 \times \mathbf{S} - \mathbf{B} + 1.47232 \times \mathbf{NHBD} + 0.03583 \times \mathbf{SOVD} - 0.67679 \times \mathbf{TD} - 717635 \times \mathbf{TVC} \quad (5)$$

$$N = 37; \ R = 0.88; \ R^2 = 0.78; R_{Ajus}^2 = 0.74; \ RMSE = 0.286; F = 21.384; \ Pr < 0.0001; R_{cv}^2 = 0.64$$

N denotes the number of compounds in the training set, while RMSE represents the root mean square error.

As a result, Fig. 2 demonstrates a strong linear correlation between the five descriptors selected and the biological activity values (pIC$_{50}$). The criteria used to evaluate the QSAR model were as follows: R^2, RMSE, F, P-value and R_{cv}^2. The higher R^2 value (0.78), lower RMSE value of 0.286, and high statistical confidence level (F = 21.384) indicate that the QSAR model is statistically acceptable. The P-value (Pr < 0.0001) shows the model's statistical significance at a level greater than 95%. S-B, NHBD, and SOVD have a positive influence, while TVC and TD have a negative influence, as shown in Fig. 3. The cross-validation correlation coefficient ($R_{cv}^2 = 0.64$) indicates the QSAR model's correctness. The MLR-based QSAR model shows a significant correlation between

observed and predicted pIC$_{50}$ values. To improve the correlation, another QSAR model will be developed using MNLR and ANN techniques.

Multiple nonlinear regression

A nonlinear QSAR model was constructed using the MNLR technique, as shown in Eq. 6

$$
\begin{aligned}
\mathbf{pIC_{50}} = {} & 14.06127 - 0.02836 \times \mathbf{S-B} + 0.48261*\mathbf{NHBD} - 1.00626 \times \mathbf{SOVD} + 5.06009 \times \mathbf{TD} - 2229421 \times \mathbf{TVC} \\
& + 0.60322 \times (\mathbf{S-B})^2 + 0.00495 \times (\boldsymbol{SOVD})^2 - 0.15036 \times (\boldsymbol{TD})^2 + 4387 \times 10^8 \times (\boldsymbol{TVC})^2
\end{aligned}
\tag{6}
$$

N = 37; R = 0.93; R^2 = 0.87; RMSE = 0.274.

The evaluation metrics of the non-linear QSAR model (R^2 = 0.87, RMSE = 0.274) demonstrate the statistical validity of this model with a p-value less than 0.05. Table 3 presents the observed and estimated biological activities for both the training and test sets using both linear and non-linear models.

MLR-QSAR modeling efficiency

Cross-validation
Figure 4 illustrates the results of cross-validation using the Leave-One-Out (LOO) approach. The results of this cross-validation (R^2 = 0.65 and RMSE = 0.31) show that cross-validation has no significant effect on the QSAR model. These clear findings demonstrate the proposed QSAR model's stability and robustness. However, it is important to note that cross-validation alone is insufficient to fully assess the capabilities of QSAR models.

Artificial neural networks
The ANN approach is employed to construct a QSAR model with a 5-3-1 architecture and a ρ value of 1.68. The ρ value between 1 and 3 indicates that the number 3 in the hidden layer is proportional to the number of descriptors 5 in the input layer, predicting the pIC$_{50}$ values represented by the output layer 1.

The QSAR model developed using the ANN approach has a very high coefficient of determination R^2 of 0.89, indicating an excellent fit to the data. Moreover, the RMSE is low (0.17), suggesting that the model predictions are highly accurate. The results demonstrate that the QSAR model is statistically reliable in predicting inhibitory activity as balanced multifunctional agents against Alzheimer's disease.

Consequently, the five descriptors (S-B, NHBD, SOVD, TVC and TD) are valuable for predicting pIC$_{50}$ values. These descriptors were selected for their relevance to this study.

Figure 5 illustrates that the predicted pIC$_{50}$ values are evenly distributed across the training set, ensuring that the ANN model predictions closely correspond to the experimentally observed pIC$_{50}$ values.

Y-randomization test
Randomization is a common strategy to ensure the reliability of QSAR models. Once a regression model is selected, Y-randomization is used to validate it. This involves shuffling the activity values of the compounds and rebuilding the model to assess its sensitivity to random variations in the data. This process is repeated 100 times to assess the model's overall robustness and identify any potential overfitting. As shown in Eq. (5), these randomized models have an average correlation coefficient of 0.36, R^2 value of 0.14 and Q_{cv}^2 of 0.63.

Random target values yielded significantly lower average R^2 and Q_{cv}^2 values compared to the model values. This suggests that the relationships between descriptors and activities in Model 1 are not coincidental, confirming the model's robustness. This randomization test validates the model's predictive power and reliability.

External validation
External validation was conducted using the Golbraikh-Tropsha criteria[68], with the aim of evaluating the ability of the QSAR models. We predicted pIC$_{50}$ activity values for compounds in the test set, as shown in Table 4. This assessment includes calculating the correlation coefficient (R^2), which is a crucial criterion for determining how effectively externally validated models can predict the activities of molecules that were not included in the model development process, as shown in Fig. 6.

The R^2 test provided a value of 0.68 with a root mean square deviation of 0.282, and all values were within the acceptable range, indicating that the Golbraikh and Tropsha criterion was successfully validated. These findings suggest that the developed QSAR model is quite successful. Furthermore, external validation of the QSAR models indicates their high capacity to reliably predict pIC$_{50}$ values for the experimental inhibitory activity of balanced multifunctional drugs against Alzheimer's disease.

Applicability domain (AD)
The William plot for the AD of the model is shown in Fig. 7.

The AD of the QSAR model was established through leverage analysis, as demonstrated by the Williams plot (Fig. 7). In the William plots. the results indicate that the leverage values of all the compounds in the training and test sets were lower than the warning leverage (h* = 0.50) except for compound 1, which was greater than the warning lever effect. This compound belongs to the training set.

The accurate prediction of the QSAR model for the test sets can be attributed to their lack of outliers. Consequently, all tested compounds fall within the AD, signifying the credibility of their predicted activity values.

Molecular docking simulations
The results shown in Fig. 8 confirm that most active ligands, C25 and C27, share common intermolecular interactions, including Trp279 amino acid residue as the active site of anti-Alzheimer's drug (1EVE.pdb), more

Comp	S-B	NHB$_D$	SOVD	TD	TVC	pIC$_{50}$Obs	MLR		MNLR	
							pIC$_{50}$Pred	Resid	pIC$_{50}$Pred	Resid
1	0.57	1	78	15	2.36E-06	5.61	5.499	0.107	5.605	0.000
2	0.22	1	80	15	1.18E-06	5.80	6.044	−0.248	5.797	−0.001
3	0.42	1	94	18	1.07E-07	6.03	5.499	0.532	5.922	0.110
4	0.53	1	96	18	7.58E-08	6.04	5.715	0.326	5.920	0.121
5	0.44	1	102	18	3.79E-08	5.97	5.857	0.113	5.793	0.177
6	0.48	1	104	18	2.68E-08	6.13	5.974	0.157	5.863	0.268
7	0.98	1	104	18	2.93E-08	6.21	6.506	−0.292	6.279	−0.065
8	0.83	1	104	20	2.93E-08	5.04	5.000	0.036	4.821	0.215
9	0.50	1	104	18	2.48E-08	5.99	5.997	−0.010	5.878	0.109
10	0.50	1	104	18	2.48E-08	6.17	5.998	0.169	5.879	0.288
11	0.50	1	104	19	2.48E-08	5.07	5.322	−0.256	5.376	−0.310
12*	0.53	1	98	18	7.44E-08	5.64	5.784	−0.147	5.829	−0.192
13	0.51	1	98	18	7.44E-08	5.53	5.761	−0.228	5.816	−0.283
14*	0.51	1	98	18	6.56E-08	5.60	5.766	−0.171	5.834	−0.239
15	0.40	1	98	18	4.64E-08	5.59	5.667	−0.079	5.821	−0.233
16	1.57	1	112	21	1.14E-08	5.37	5.414	−0.043	5.308	0.062
17	1.00	1	112	21	9.61E-09	4.31	4.802	−0.492	4.442	−0.132
18	1.33	1	112	19	1.14E-08	6.70	6.515	0.184	6.811	−0.112
19	0.89	1	112	19	1.04E-08	5.92	6.044	−0.127	6.234	−0.317
20	0.87	1	112	19	9.61E-09	6.46	6.013	0.443	6.205	0.251
21	1.06	1	112	19	1.04E-08	6.48	6.221	0.261	6.424	0.058
22	0.62	1	112	19	9.47E-09	6.20	5.750	0.450	5.993	0.208
23*	0.59	1	112	19	8.77E-09	5.64	5.719	−0.080	5.973	−0.335
24	0.97	2	120	20	2.59E-09	7.07	7.211	−0.146	7.148	−0.083
25	0.53	2	120	20	2.37E-09	6.43	6.740	−0.308	6.764	−0.332
26	0.50	2	120	20	2.19E-09	7.16	6.708	0.453	6.746	0.415
27	0.98	1	106	18	2.54E-08	6.55	6.584	−0.031	6.358	0.195
28	0.54	1	106	18	2.32E-08	5.78	6.115	−0.332	5.973	−0.191
29*	0.51	1	106	18	2.15E-08	6.05	6.084	−0.034	5.959	0.091
30*	1.00	1	106	18	2.54E-08	6.60	6.603	−0.001	6.379	0.223
31	0.56	1	106	18	2.32E-08	6.06	6.133	−0.078	5.984	0.071
32	0.53	1	106	18	2.15E-08	5.59	6.102	−0.512	5.969	−0.379
33*	0.98	1	106	18	2.88E-08	6.13	6.588	−0.457	6.357	−0.226
34	0.51	1	106	18	2.44E-08	5.84	6.088	−0.244	5.956	−0.112
35	0.97	1	112	18	9.61E-09	6.80	6.805	−0.009	6.825	−0.029
36	0.53	1	112	18	8.77E-09	6.24	6.335	−0.091	6.440	−0.196
37	0.50	1	112	18	8.12E-09	6.60	6.303	0.299	6.423	0.179
38	1.00	1	112	19	1.89E-09	6.34	6.165	0.172	6.373	−0.035
39	0.56	1	122	19	1.73E-09	5.94	6.053	−0.118	7.492	−1.556
40	0.53	1	122	19	1.60E-09	6.00	6.022	−0.022	7.473	−1.473
41	1.28	1	112	20	1.14E-08	5.67	5.778	−0.112	5.920	−0.254
42	1.04	1	112	20	1.04E-08	5.80	5.525	0.274	5.597	0.201
43	0.97	1	112	19	9.61E-09	5.93	6.130	−0.201	6.323	−0.395
44*	1.38	1	116	21	5.68E-09	4.78	5.353	−0.571	5.471	−0.689
45*	1.01	2	124	22	1.30E-09	5.57	6.045	−0.479	5.494	0.071
46*	1.47	1	112	21	1.14E-08	5.66	5.311	0.351	5.135	0.526

Table 3. The biological activities predicted by the QSAR model, using both training and test sets.

than Asp72 and Tyr334 amino acids residues. These interactions were all detected with the lowest possible binding energies in kcal/mol, -7.26 and -6.1 kcal/mol, respectively. The novel-designed compound, labeled Pred12, which was predicted in the current study with the highest acetylcholinesterase inhibitory activity based on the validated QSAR model, was equally docked to the same targeted receptor (1EVE.pdb). The docking results revealed similar intermolecular interactions, such as Trp84 and Trp279 amino acid residues as two active sites of the targeted protein, in addition to other common chemical bonds produced towards Tyr334 and Phe330 amino acid residues. One additional hydrogen bond was detected towards the Phe288 amino acid
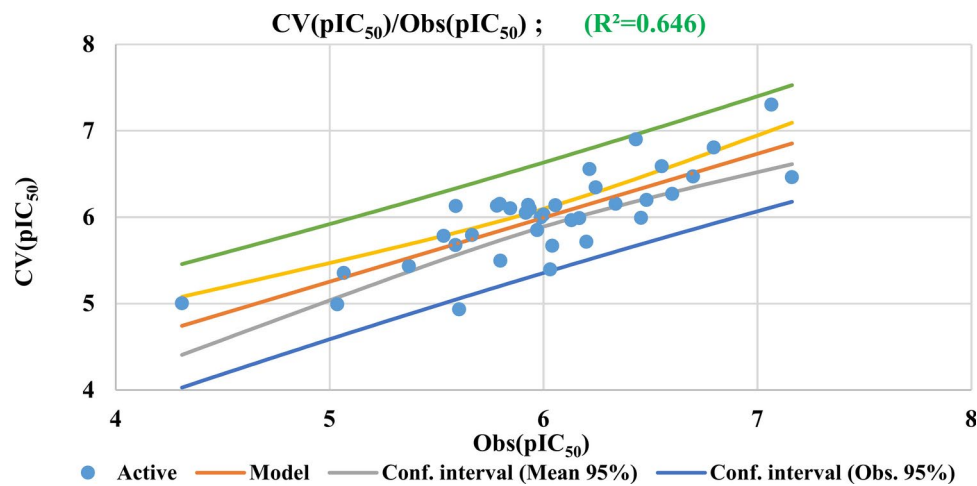
Fig. 4. Correlation of observed and predicted activities calculated using LOO-CV.
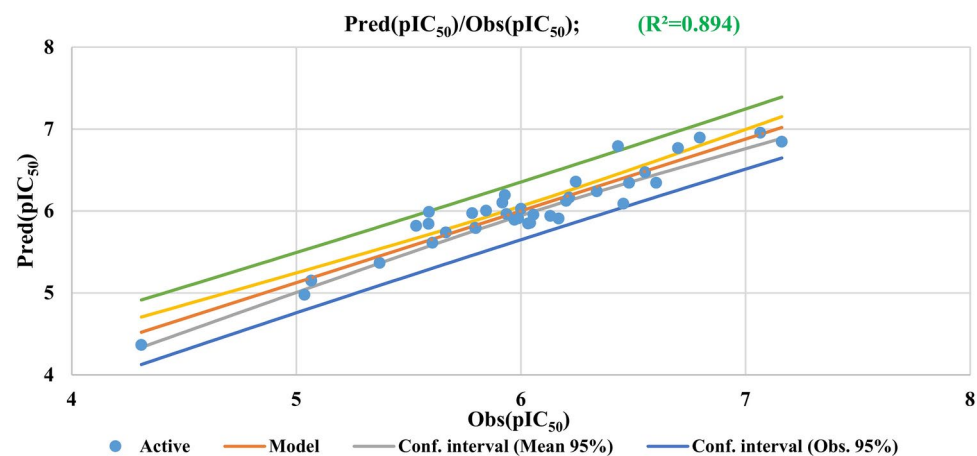

Fig. 5. Correlation between the observed and the predicted activities calculated by ANN.

Compounds	Obs(pIC_{50}) MLR	Pred (pIC_{50}) MLR	Residual
12	5.63639	5.784	-0.147
14	5.59517	5.766	-0.171
23	5.63827	5.719	-0.080
29	6.05061	6.084	-0.034
30	6.60206	6.603	-0.001
33	6.13077	6.588	-0.457
44	4.78252	5.353	-0.571
45	5.56543	6.045	-0.479
46	5.66154	5.311	0.351

Table 4. The results of the prediction by MLR methods for the test set.

residue, making the novel-designed compound highly stable in terms of energy order (binding energy of -7.94 kcal/mol)[73]. Moreover, the molecular docking protocol has been successfully validated[29,70] as the candidate ligands labeled C25 and C27 more than most active molecules from the newly designed compounds marked Pred12 were effectively docked to two active sites of the three-dimensional structure of the anti-Alzheimer drug complexed with its target acetylcholinesterase co-crystallized ligand as shown in Fig. 9.
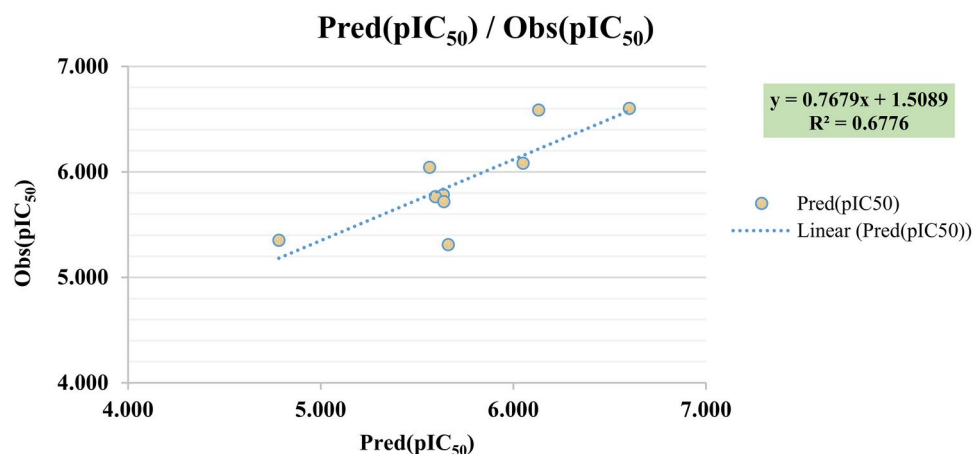
Fig. 6. Correlations between the observed/predicted activity by the MLR model for the test set.
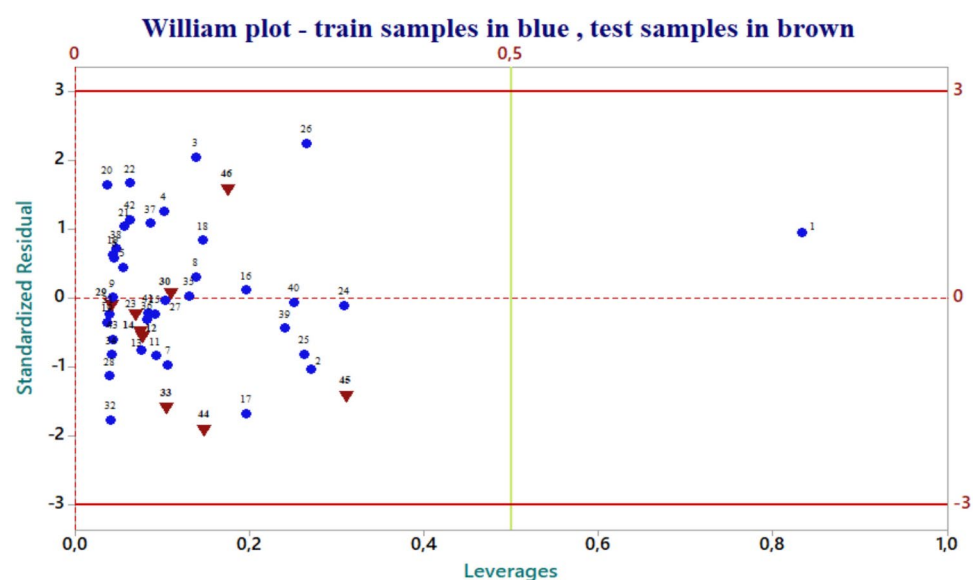

Fig. 7. The Williams graph of the model presented by Eq. (5).

*MD simulation*

The complexes of the human AChE receptor complexed with ligands 61, 726, and 794 were selected for MD simulation to evaluate their thermodynamic stability over a 100 ns timescale. A stable drug-receptor complex is essential for exerting a therapeutic response. The macromolecular complex underwent a 100 ns MD simulation using Schrodinger's Desmond software version 2022.4. The target AChE receptor's monomeric chain consists of 534 amino acids, comprising 4254 heavy atoms out of a total of 8369 atoms. To assess thermodynamic stability, structural changes and root-mean-square deviation (RMSD) analysis of the macromolecular backbone were performed throughout the 100 ns simulation. Ligand 61, with thirteen flexible bonds and thirty-four heavy atoms out of seventy-two total, displayed high stability in complex with human AChE throughout the simulation. The RMSD value of the receptor's backbone fluctuated between 1.2 and 2.4 Å, while the bound ligand 61 exhibited minor RMSD fluctuations within the receptor cavity. ranging from 3.0 to 5.0 Å.

RMSF analysis, which measures the deviation of atoms from their initial positions, is a crucial parameter for assessing the flexibility and dynamic behavior of the macromolecular complex. To assess protein dynamics and stability, RMSF analysis was conducted on the human AChE receptor complexed with ligand 61. The MD simulation results showed that the RMSF values for the Cα backbone remained within a stable range of 0.5–2.5 Å, except for a few terminal residues, while for ligand 61, it was found to be ranging from 1.0 to 2.0 Å. RMSF of human AChE receptor's backbone and complexed ligand 61, observed during MD analysis, is depicted in Fig. 10.

The stability of the receptor-ligand complexes was evaluated by monitoring hydrophobic contacts, ionic interactions and hydrogen bonds formed during MD simulations. Ligand 61 interacted with the human AChE receptor via hydrophobic contacts with Tyr70, Trp84, Tyr121, Trp279, Leu282, Phe330 and Phe331. Additionally,
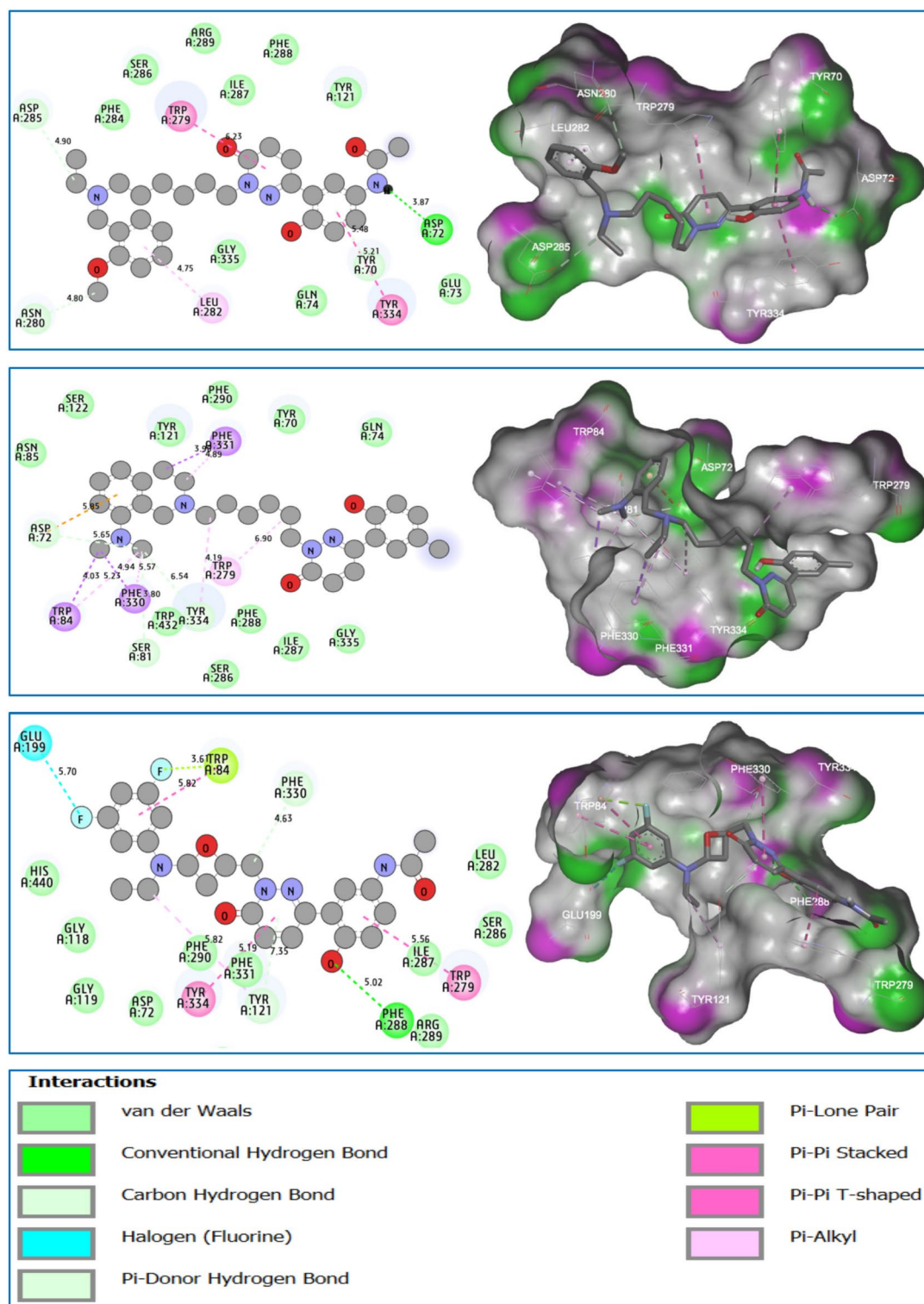
Fig. 8. Intermolecular contacts in two and three dimensions between 1EVE.pdb protein and C25. C27. and Pred12 with binding energies of − 7.26. − 6.1. and − 7.94 kcal/mol. respectively.

hydrogen bonds formed with Tyr121, Phe284, Asp285, Ser286, Phe288 and Arg289 while Trp279 and Ser286 interacted through water bridges.

In another simulation, the complexed ligand 726 complexed with the human AChE enzyme, revealed that it constitutes fifteen flexible bonds, comprising thirty-six heavy atoms of seventy-two atoms in total. The human AChE-ligand 726 conjugate has displayed high stability throughout the simulation. RMSD (Root Mean Square Deviation) analysis revealed that the receptor's backbone exhibited fluctuations between 1.2 and 2.1 Å during
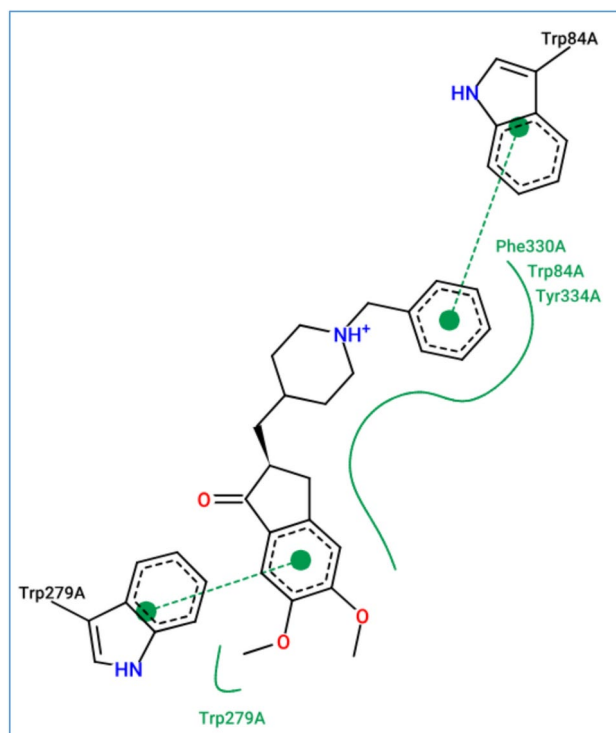
Fig. 9. Active sites of the targeted receptor encoded in PDB basis by 1EVE.pdb.

the simulation. The bound ligand 726 also showed minor fluctuations within the receptor cavity. ranging from 3.2 to 7.0 Å. Molecular dynamics simulations of the human AChE receptor complexed with ligand 726 revealed the RMSF (Root Mean Square Fluctuation) for the Cα backbone remained within 0.5–2.0 Å, except for some terminal residues, while for ligand 726, it was found to be ranging from 1.0 to 4.0 Å. The RMSF of human AChE receptor's backbone and complexed ligand 726, observed during MD analysis, is depicted in Fig. 11. Throughout the simulation, ligand 726 was found to be interacting with human AChE receptor via the formation of hydrophobic bonds with the amino acids Tyr70, Phe75, Trp279, Phe290, Phe331, Tyr334, Pro337, Leu358 whereas Tyr70, Val71, Asp72, Trp84, Tyr121, Phe288, Arg289 and Tyr334 interacted via hydrogen bonds. Additionally, the amino acid Tyr70, Trp84, Asp285 and Tyr334 formed water bridges.

MD simulation of the ligand complex 794, complexed with the human AChE enzyme, revealed that it constitutes nine flexible bonds, comprising thirty-four heavy atoms of fifty-eight atoms in total. The human AChE-ligand 794 conjugate has displayed high stability throughout the simulation. The RMSD value of the receptor's backbone was found to fluctuate between 1.0 and 1.75 Å, whereas the bound ligand 794 exhibited minor fluctuations in its RMSD value within the receptor cavity, ranging from 3.6 to 5.0 Å. Figure 12 illustrates the root-mean-square deviation (RMSD) profiles for human AChE receptor complexes with ligands 61, 726 and 794 respectively.

Molecular dynamics (MD) simulations of the AChE-ligand 794 complex revealed that the RMSF for the Cα backbone remained within 0.5–2.0 Å for most residues, except for a few terminal residues, while for ligand 794, it was found to be ranging from 1.0 to 3.0 Å. The RMSF of the human AChE receptor's backbone and complexed ligand 794, observed during MD analysis, is depicted in Fig. 13.

Throughout the simulation, ligand 794 was found to be interacting with the human AChE receptor via formation of hydrophobic bonds with the amino acids Met83, Trp84, Tyr121, Trp279, Phe288, Phe290, Phe330, Phe331, Tyr334 and His440. Additionally, hydrogen bonds were formed with Tyr70, Glu73, Gln74, Tyr121 and Ser122 while the amino acid Gln69, Tyr70, Val71, Asp72, Gln74, Tyr121, Phe288, Arg289 and Tyr334 interact via water bridges. Figure 14 shows the interactions of ligand 61 (a), ligand 726 (b) and ligand 794 (c) with human AChE receptor residues.

Design of new compounds
Table 5 presents the predicted values of molecular descriptors and pIC$_{50}$ activities, calculated using the multiple linear regression study, which was used to develop a quantitative structure–activity relationship model for predicting the inhibitory activity of pyridazin-3(2H)-one derivatives against Alzheimer's disease. The model was built using a dataset of compounds with known inhibitory activity, and the selected descriptors were calculated using molecular modeling software. The MLR model showed good statistical performance, with a high coefficient of determination (R^2) and low root mean square error (RMSE) values.

The primary goal of this research is to develop novel Alzheimer's disease inhibitors derived from pyridazin-3(2H)-one, using the suggestions obtained from the 2D-QSAR investigations. In this work, thirteen pyridazin-
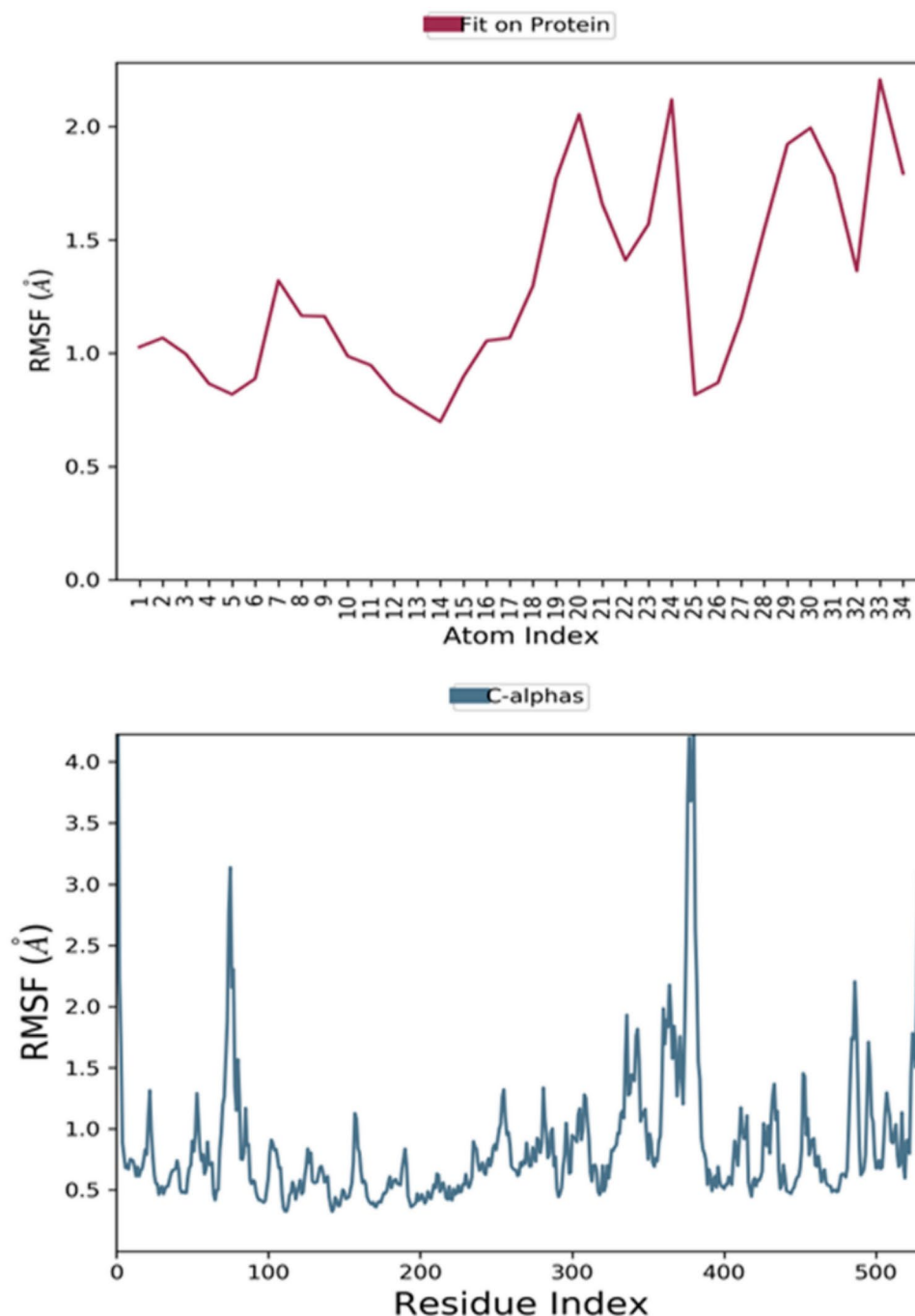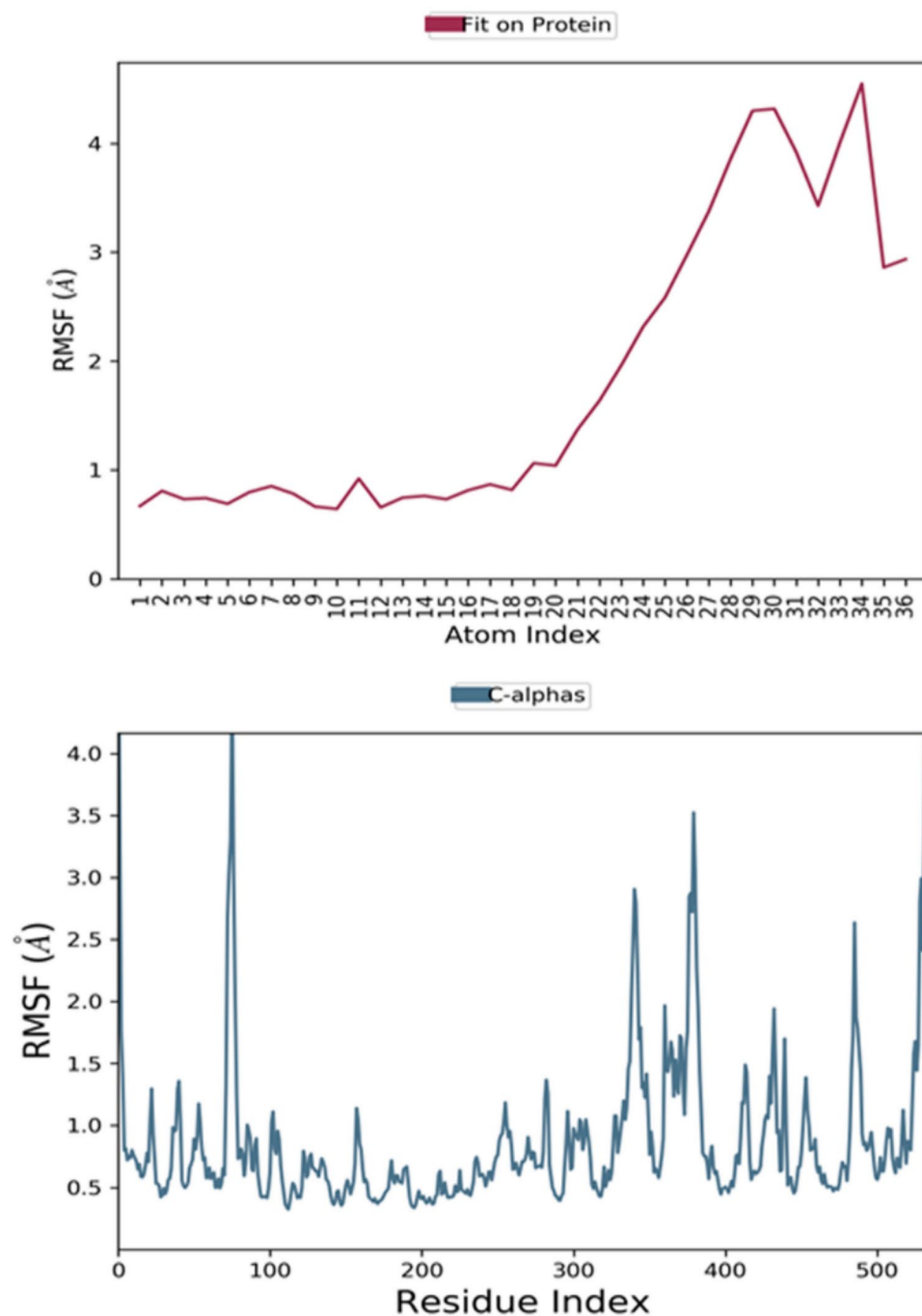
Fig. 10. RMSF for Cα chain of human AChE complexed with ligand 61 detected while executing 100ns MD simulation.

3(2H)-one derivatives (Pred1–Pred13) were designed to improve the inhibitory efficacy against Alzheimer's disease (Table 6). To evaluate the potential of the newly proposed compounds, we used the same molecular descriptors as those used for the existing series of molecules. We then applied the MLR model (a regression analysis method) to predict their activity. The results presented in Table 8 indicate that these novel compounds exhibit comparable or superior inhibitory activity to the most active compounds in the series. This suggests their potential as promising candidates for Alzheimer's disease treatment.

Lipinski's rule
A potent drug is a chemical substance that has successfully passed several screening phases. Most drugs fail in preclinical testing because they lack the unique characteristics needed to be considered drug candidates. ADMET evaluation, an essential parameter in drug development, is of great importance in the early stages to reduce the failure rate of drug candidates.

Fig. 11. RMSF for Cα chain of human AChE complexed with ligand 726 detected while executing 100ns MD simulation.

In our study, Thirteen predicted molecules were subjected to in-silico ADMET testing, and all showed a high probability of being absorbed in the gut, as shown in Table 8. Those molecules that penetrate the gut also have a marked tendency to be absorbed by the human organism. An in vivo study confirmed that these 13 predicted molecules could effectively improve cognitive dysfunction in scopolamine-treated individuals by regulating acetylcholine levels and inhibiting oxidative stress. These results highlight the potential of these predicted molecules as novel, balanced candidates for the pharmacotherapy of Alzheimer's disease.

Next, we assessed the drug-like physicochemical properties of the 13 predicted molecules with the aim of determining their potential for administration as drugs. Using Lipinski's rule as a benchmark, these compounds met the criteria and fulfilled the topological polar surface area (TPSA) requirements for central nervous system drugs (Table 7)[71]. In addition, the thirteen predicted molecules were expected to have moderate water solubility and good gastrointestinal absorption capacity. Consequently, we concluded that these 13 predicted molecules possessed favorable physicochemical properties like those of drugs.
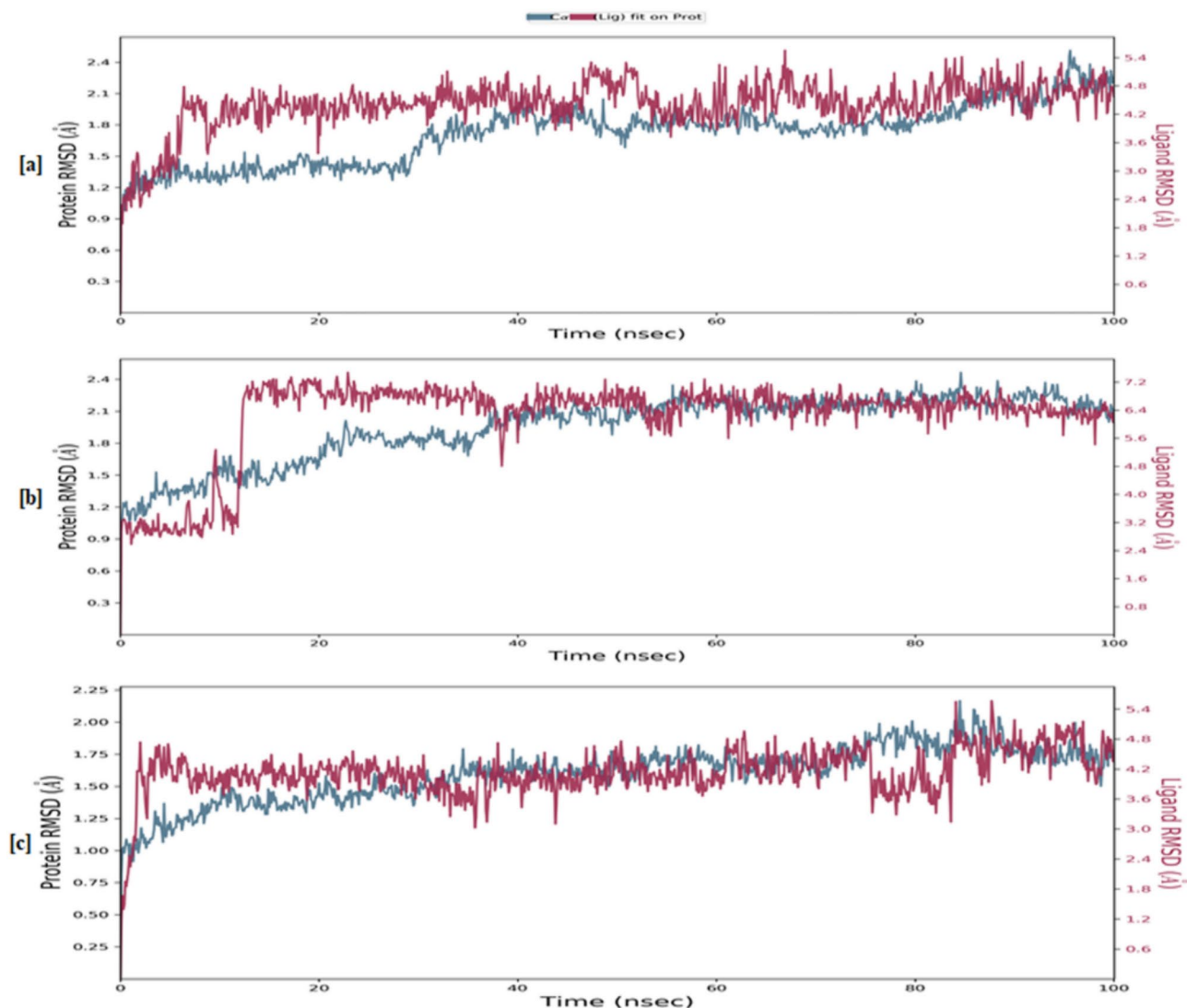
Fig. 12. RMSD for Cα chain of human AChE complexed with ligand 61 (**a**), ligand 726 (**b**) and ligand 794 (**c**) detected while executing 100ns MD simulation.

ADMET properties

To ensure the potential relevance of molecules designed as drugs, we took into account pharmacokinetic parameters such as ADMET. In silico ADMET properties were predicted using the pkCSM online tool[72], and the details are provided in the corresponding table (Table 8).

Absorption levels below 30% indicate poor absorption, while values above 90% indicate acceptable absorption in the human digestive system. It is important to note that a volume of distribution (VDss) greater than 0.45 is considered significant. The predicted compounds demonstrated excellent intestinal absorption, suggesting widespread distribution throughout the body. Enzymatic metabolism, the biochemical transformation of drugs in the body, plays a crucial role in modifying pharmacological molecules. This process can generate various metabolites that influence drug responses to varying degrees[73]. Given the potential differences in physicochemical and pharmacological properties, a thorough investigation of drug metabolism is essential.

Cytochrome P450 (CYP450) enzymes, particularly those in the CYP1, CYP2, CYP3, and CYP4 families, are responsible for over 90% of phase I metabolism. Among these, CYP3A4 is especially relevant to our research, as the novel compounds we developed act as both substrates and inhibitors of this enzyme[75].

Clearance, a measure of how quickly a drug is eliminated from the body, is influenced by various factors. The newly discovered compounds exhibited notably high clearance values, ensuring optimal drug retention. Additionally, assessing the non-toxicity of predicted molecules is a critical step in drug selection. Further investigations are necessary to evaluate the toxicity profiles of these compounds. Fortunately, all the molecules we developed are non-toxic, adding to their potential as drug candidates.

In the pursuit of developing drug candidates for Alzheimer's disease, the focus has been on inhibiting self-induced $A\beta_{1-42}$ aggregation and self-induced $A\beta_{1-42}$ fibril disaggregation. However, as reported in the 2022 study by Yichun et al., certain limitations have been observed in the development of synthetic drugs targeting
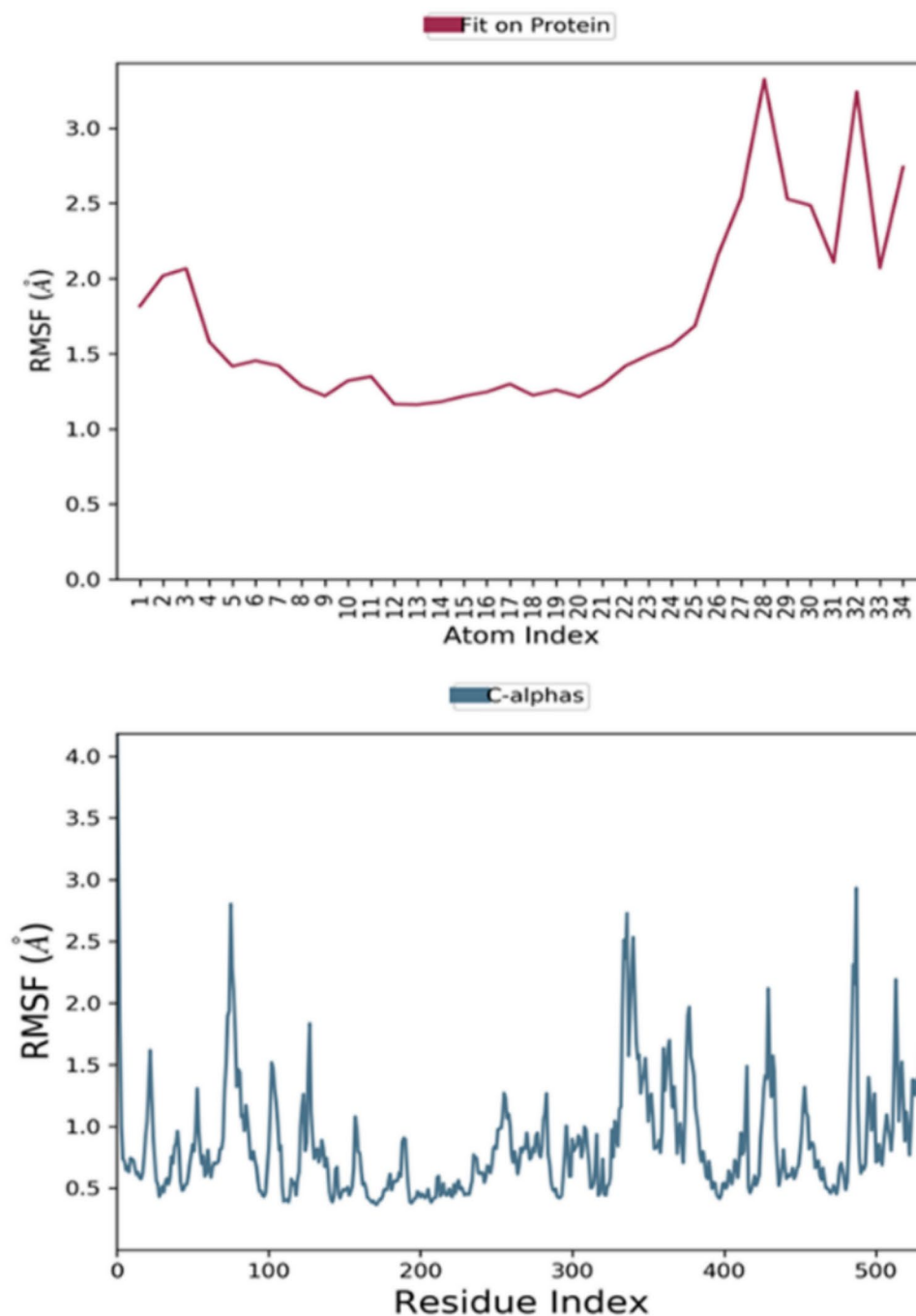
Fig. 13. RMSF for Cα chain of human AChE complexed with ligand 794 detected while executing 100ns MD simulation.

these processes. These limitations include the inability to cross the blood–brain barrier (BBB), safety profile issues, limited solubility, and undesirable side effects. Therefore, addressing these challenges is essential in the development of novel drug candidates for Alzheimer's disease.

These findings emphasize the importance of the predicted molecules for the development of dual-binding AChE inhibitors targeting both the PAS and the catalytic active site (CAS) of AChE, which could offer multiple activities against AChE, Aβ and delay the progression of AD.

Conclusion

In conclusion, this study aimed to develop new pyridazine-derived drugs as innovative multifunctional agents against Alzheimer's disease. A 2D-QSAR analysis was performed to investigate the structural factors influencing the biological activity of 46 pyridazine-derived analogs acting as AD inhibitors. The MLR analysis method used to build the QSAR model demonstrated strong predictive power, indicating its reliability in predicting
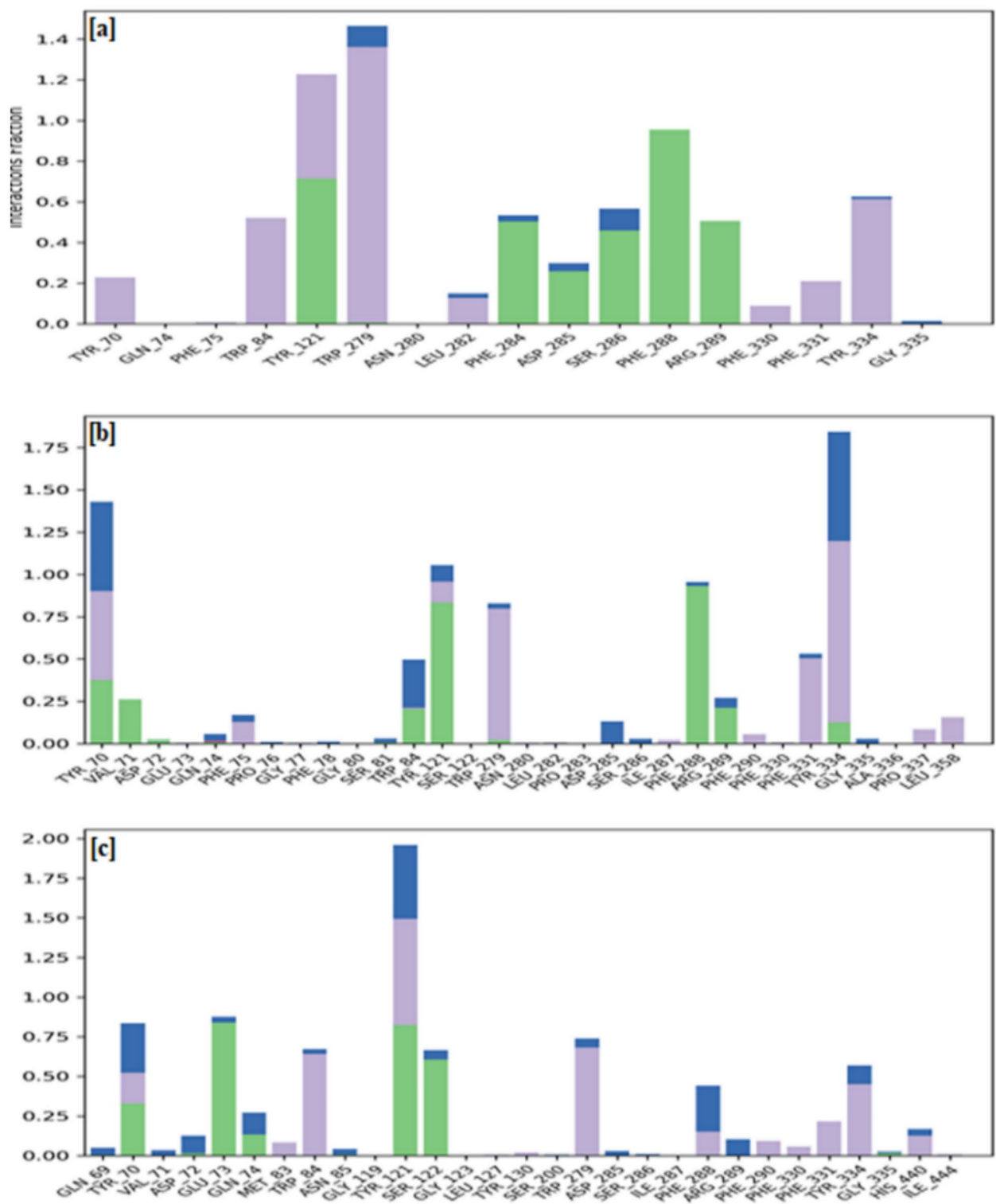
Fig. 14. Protein–Ligand Contacts: Protein–ligand interactions identified between the human AChE receptor and ligand 61 (**a**), ligand 726 (**b**) and ligand 794 (**c**) respectively. The interactions were visualized using different colored bars with green representing h.

the biological inhibitory activity of the $A\beta_{1-42}$ receptor. The developed QSAR model equation revealed five key descriptors (Stretch-Bend, Number of Hydrogen Donor Bonds, Sum of Valence Degrees, Total Valence Connectivity, and Topological Diameter) that significantly influence the biological inhibitory activity of the $A\beta_{1-42}$ receptor. These findings emphasize the importance of these descriptors in designing potent compounds

Comp	S-B	NHBD	SOVD	TD	TVC	pIC$_{50}$–pred
Comp 26	0.50	20	120	20	2.19×10^{-9}	7.16
Pred1	0.7447	2	124	19	1.70×10^{-9}	7.79
Pred2	0.7196	2	122	18	2.40×10^{-9}	8.37
Pred3	0.724	2	114	18	7.34×10^{-9}	8.08
Pred4	0.3923	2	114	17	6.20×10^{-9}	8.41
Pred5	− 1.3624	2	130	17	5.52×10^{-10}	7.10
Pred6	− 0.3483	2	118	17	2.92×10^{-9}	7.76
Pred7	0.1195	2	118	18	3.46×10^{-9}	7.58
Pred8	0.1129	2	126	18	1.13×10^{-9}	7.86
Pred9	0.3101	2	130	18	6.54×10^{-10}	8.22
Pred10	0.3222	2	122	18	2.00×10^{-9}	7.94
Pred11	− 0.059	2	122	17	1.69×10^{-9}	8.21
Pred12	− 0.0682	2	130	17	5.52×10^{-10}	8.49
Pred13	− 0.0908	2	138	18	1.81×10^{-10}	8.08

Table 5. The values of parameters calculated for the news molecules and their predicted activities.

for developing dual binding site AChEIs targeting both the PAS and the catalytic active site (CAS) of AChE, offering multiple activities against AChE, Aβ and delaying the progression of AD.

Based on the MLR equation analysis, thirteen new molecules with more potent activity were developed. Evaluation of the pharmacokinetic properties of these selected molecules revealed acceptable characteristics, and an in-silico assessment of their ADMET properties indicated favorable pharmacokinetic profiles. These molecules show potential as valuable new agents in combating Alzheimer's disease by effectively inhibiting A$\beta_{1\text{-}42}$ aggregation and enzymatic activity.

The information presented in this study offers medicinal chemists numerous possibilities for developing drugs as more potent balanced multifunctional agents against Alzheimer's disease by using the molecular structure of these compounds to design new derivatives with enhanced activities.

In future research, we plan to develop 3D-QSAR models based on the pyridazine derivative series to further improve the design and development of potential Alzheimer's disease therapies.

Compds	Structure	Bioavailability radars	EGG BILLED	pIC$_{50}$pred
Comp 26				7.16
Pred1				7.79
Pred2				8.37
Pred3				8.08
Pred4				8.41
Pred5				7.10
Pred6				7.76

Table 6. Structures of new compounds and their pIC$_{50}$ predicted based on the 2D-QSAR model.
EGG BILLED: The white area represents the physico-chemical space of molecules with the highest probability of absorption in the gastrointestinal tract, the yellow area (egg yolk) is the physico-chemical space of molecules with the highest probability of brain penetration.
Bioavailability radars: the pink area represents the optimal range for each ingredient.

Pred7				7.58
Pred8				7.86
Pred9				8.22
Pred10				7.94
Pred11				8.21
Pred12				8.49
Pred13				8.08

Table 6. (continued)

	TPSA	n-Rotatable bonds	MW	LogP	n-HBA	n-HBD	Violations Lipinski	Veber	Egan	Muegge	Synthetic accessibility
Rule	< 140 A^2	< 10	< 500 D.a	≤ 5	< 10	< 5	≤ 2	≤ 2	≤ 2	≤ 2	0 < S.A < 10
Compd 26	87.46	12	480.584	4.7959	6	2	Yes	No	Yes	Yes	3.66
Pred1	90.70	11	495.599	4.0817	7	2	Yes	No	Yes	Yes	3.83
Pred2	90.70	10	481.572	3.6916	7	2	Yes	No	Yes	Yes	3.76
Pred3	90.7	10	463.582	3.5525	7	2	Yes	No	Yes	Yes	3.72
Pred4	87.46	9	438.503	3.6256	6	2	Yes	Yes	Yes	Yes	3.41
Pred5	99.99	8	470.476	3.1464	7	2	Yes	Yes	Yes	Yes	4.29
Pred6	87.46	7	450.514	4.0185	6	2	Yes	Yes	Yes	Yes	4.16
Pred7	90.70	8	475.593	3.9454	7	2	Yes	No	Yes	Yes	4.55
Pred8	90.70	8	493.583	4.0845	7	2	Yes	Yes	Yes	Yes	4.56
Pred9	99.93	8	495.555	3.4209	8	2	Yes	Yes	Yes	Yes	4.81
Pred10	99.93	8	477.565	3.2818	8	2	Yes	Yes	Yes	Yes	4.80
Pred11	96.69	7	452.486	3.3549	7	2	Yes	Yes	Yes	Yes	4.42
Pred12	96.69	7	470.476	3.494	7	2	Yes	Yes	Yes	Yes	4.43
Pred13	96.69	7	488.466	3.6331	7	2	Yes	Yes	Yes	Yes	4.43

Table 7. Lipinski's role of newly designed compounds and and there Drug-like properties.

Models	Absorption: Intestinal absorption (human) Numeric (%absorbed)	P-Gp substrate Categorical (yes/no)	Distribution: VDss (human) Numeric (Log L kg^{-1})	BBB permeability Numeric (Log BB)	CNS permeability Numeric (Log PS)	Metabolism CYP450 Substrate 2D6	3A4	Inhibitor 1A2	2C19	2C9	2D6	3A4	Excretion: Total clearance Numeric (log mL min^{-1} kg^{-1})	Toxicity: AMES toxicity Categorical (yes/no)
Comp 26	90.734	Yes	1.427	− 1.48	− 2.692	No	Yes	No	Yes	Yes	No	Yes	0.757	No
Pred1	92.512	Yes	1.476	− 1.478	− 2.792	No	Yes	No	No	Yes	No	Yes	0.585	No
Pred2	92.752	Yes	1.408	− 1.439	− 2.78	No	Yes	No	No	Yes	No	Yes	0.522	No
Pred3	92.511	Yes	1.332	− 1.227	− 2.727	No	Yes	No	No	Yes	No	Yes	0.623	No
Pred4	92.299	Yes	1.264	− 1.375	− 1.375	No	Yes	No	Yes	Yes	No	Yes	0.582	No
Pred5	91.329	yes	0.494	− 1.289	− 3.58	No	No	No	No	Yes	No	Yes	0.492	No
Pred6	95.394	Yes	0.792	− 0.866	− 2.446	No	Yes	No	No	Yes	No	Yes	0.338	No
Pred7	95.551	Yes	0.798	− 0.797	− 2.483	No	Yes	No	Yes	Yes	No	Yes	0.793	No
Pred8	95.737	yes	0.8	− 1	− 2.527	No	Yes	No	Yes	Yes	No	Yes	0.335	No
Pred9	93.907	Yes	0.638	− 1.212	− 3.246	No	Yes	No	Yes	Yes	No	Yes	0.423	No
Pred10	93.559	Yes	0.63	− 1.006	− 2.695	No	Yes	No	Yes	Yes	No	Yes	0.768	No
Pred11	96.463	yes	0.642	− 1.078	− 3.219	No	Yes	No	Yes	Yes	No	Yes	0.265	No
Pred12	94.643	Yes	0.548	− 1.28	− 2.994	No	Yes	No	Yes	Yes	No	Yes	0.438	No
Pred13	90.724	Yes	90.724	− 1.476	− 3.018	No	Yes	No	Yes	Yes	No	Yes	0.37	No

Table 8. ADMET properties of the lead molecules in the dataset.

Data availability

All data generated or analysed during this study are included in this published article.

References

1. da Silva, C. T. P., Carvalho, I. & Taft, C. A. Homology modeling and molecular interaction field studies of α-glucosidases as a guide to structure-based design of novel proposed anti-HIV inhibitors. *J. Comput. Aided Mol. Des.* **19**, 83–92 (2005).
2. Schneider, G. & Fechner, U. Computer-based de novo design of drug-like molecules. *Nat. Rev. Drug Discov.* **4**, 649–663 (2005).
3. da Silva, C. H. T. P., Campo, V. L., Carvalho, I. & Taft, C. A. Molecular modeling, docking and ADMET studies applied to the design of a novel hybrid for treatment of Alzheimer's disease. *J. Mol. Graph. Model.* **25**, 169–175 (2006).

4. Suman, R., et al. CSIR-National Institute of Science Communication and Policy Research (CSIR-NIScPR) (2023).
5. Kocahan, S. & Doğan, Z. Mechanisms of Alzheimer's disease pathogenesis and prevention: The brain, neural pathology, N-methyl-D-aspartate receptors, tau protein and other risk factors. *Clin. Psychopharmacol. Neurosci.* **15**, 1–8 (2017).
6. Reichman, W. E. Current pharmacologic options for patients with Alzheimer's disease. *Ann. Gen. Hosp. Psychiatry* **2**, 1 (2003).
7. WorldAlzheimerReport2019-French-Summary.pdf.
8. International, A. D. World Alzheimer Report 2019: Attitudes to dementia (2019).
9. Cummings, J., Lee, G., Ritter, A., Sabbagh, M. & Zhong, K. Alzheimer's disease drug development pipeline: 2020. *Alzheimers Dement. Transl. Res. Clin. Interv.* **6**, e12050 (2020).
10. Lee, J. et al. Prevalence of dementia in India: National and state estimates from a nationwide study. *Alzheimers Dement. J. Alzheimers Assoc.* **19**, 2898–2912 (2023).
11. Donepezil: An anticholinesterase inhibitor for Alzheimer's disease | American Journal of Health-System Pharmacy | Oxford Academic. https://academic.oup.com/ajhp/article-abstract/54/24/2805/5158531
12. Role of cholinergic signaling in Alzheimerrsquos disease. https://www.mdpi.com/1420-3049/27/6/1816
13. The Cholinesterases: From Genes to Proteins. *Ann. Rev.* https://doi.org/10.1146/annurev.pa.34.040194.001433
14. Shi, Y. et al. Development of novel 2-aminoalkyl-6-(2-hydroxyphenyl)pyridazin-3(2H)-one derivatives as balanced multifunctional agents against Alzheimer's disease. *Eur. J. Med. Chem.* **230**, 114098 (2022).
15. Giacobini, E. Cholinergic foundations of Alzheimer's disease therapy. *J. Physiol. Paris* **92**, 283–287 (1998).
16. Wakulik, K. et al. Effect of novel pyrrolo[3,4-d]pyridazinone derivatives on lipopolysaccharide-induced neuroinflammation. *Int. J. Mol. Sci.* **21**, 2575 (2020).
17. Gökçe, M., Utku, S. & Küpeli, E. Synthesis and analgesic and anti-inflammatory activities 6-substituted-3(2H)-pyridazinone-2-acetyl-2-(p-substituted/nonsubstituted benzal)hydrazone derivatives. *Eur. J. Med. Chem.* **44**, 3760–3764 (2009).
18. Cao, X. et al. Synthesis and biological evaluation of novel σ1 receptor ligands for treating neuropathic pain: 6-hydroxypyridazinones. *J. Med. Chem.* **59**, 2942–2961 (2016).
19. Contreras, J.-M., Rival, Y. M., Chayer, S., Bourguignon, J.-J. & Wermuth, C. G. Aminopyridazines as acetylcholinesterase inhibitors. *J. Med. Chem.* **42**, 730–741 (1999).
20. Approches synthétiques des nouveaux médicaments approuvés en 2017. *J. Med. Chem.* https://doi.org/10.1021/acs.jmedchem.9b00196
21. Berkenstam, A. & Gustafsson, J. -Å. Nuclear receptors and their relevance to diseases related to lipid metabolism. *Curr. Opin. Pharmacol.* **5**, 171–176 (2005).
22. Ligands à cibles et à la direction pour lutter contre les maladies neurodégénératives. J. Med. Chem. https://doi.org/10.1021/jm7009364
23. Ramos, D. et al. Mimicking microvascular alterations of human diabetic retinopathy: A challenge for the mouse models. *Curr. Med. Chem.* **20**, 3200–3217 (2013).
24. Alzheimer's disease drug development pipeline: 2019-Cummings-2019-Alzheimer's & Dementia: Translational Research & Clinical Interventions. Wiley Online Library. https://doi.org/10.1016/j.trci.2019.05.008
25. Huang, Y. & Mucke, L. Alzheimer mechanisms and therapeutic strategies. *Cell* **148**, 1204–1222 (2012).
26. Chakrovorty, A., Bhattacharjee, B., Saxena, A., Samadder, A. & Nandi, S. Current naturopathy to combat Alzheimer's disease. *Curr. Neuropharmacol.* **21**, 808–841 (2023).
27. Yamari, I. et al. The anticoagulant potential of *Lippia Alba* extract in inhibiting SARS-CoV-2 Mpro: Density functional calculation, molecular docking analysis, and molecular dynamics simulations. *Sci. Afr.* **23**, e01986 (2024).
28. Aloui, M. et al. QSAR modelling, molecular docking, molecular dynamic and ADMET prediction of pyrrolopyrimidine derivatives as novel Bruton's tyrosine kinase (BTK) inhibitors. *Saudi Pharm. J.* **32**, 101911 (2024).
29. El Fadili, M. et al. QSAR, ADMET in silico pharmacokinetics, molecular docking and molecular dynamics studies of novel bicyclo (aryl methyl) benzamides as potent GlyT1 inhibitors for the treatment of schizophrenia. *Pharmaceuticals* **15**, 670 (2022).
30. Er-rajy, M. et al. 2D-QSAR modeling, drug-likeness studies, ADMET prediction, and molecular docking for anti-lung cancer activity of 3-substituted-5-(phenylamino) indolone derivatives. *Struct. Chem.* **33**, 973–986 (2022).
31. Er-rajy, M. et al. Design of novel anti-cancer agents targeting COX-2 inhibitors based on computational studies. *Arab. J. Chem.* **16**, 105193 (2023).
32. Österberg, T. & Norinder, U. Prediction of drug transport processes using simple parameters and PLS statistics. The use of ACD/logP and ACD/ChemSketch descriptors. *Eur. J. Pharm. Sci.* **12**, 327–337 (2001).
33. Milne, G. W. A. Software review of ChemBioDraw 12.0. *J. Chem. Inf. Model.* **50**, 2053–2053 (2010).
34. Parr, R. G. & Yang, W. Density-functional theory of the electronic structure of molecules. *Annu. Rev. Phys. Chem.* **46**, 701–728 (1995).
35. Zhang, Y., Xu, X. & Goddard, W. A. Doubly hybrid density functional for accurate descriptions of nonbond interactions, thermochemistry, and thermochemical kinetics. *Proc. Natl. Acad. Sci.* **106**, 4963–4968 (2009).
36. Frisch, M. J. et al. Gaussian 03, Revision C. 02. Wallingford, CT: Gaussian. *IncGoogle Sch.* (2004).
37. Aloui, M. et al. Design of novel potent selective survivin inhibitors using 2D-QSAR modeling, molecular docking, molecular dynamics, and ADMET properties of new MX-106 hydroxyquinoline scaffold derivatives. *Heliyon* **10**, e38383 (2024).
38. Roy, K. & Mitra, I. On various metrics used for validation of predictive QSAR models with applications in virtual screening and focused library design. *Comb. Chem. High Throughput Screen.* **14**, 450–474 (2011).
39. Er-rajy, M., El fadili, M., Mrabti, N. N., Zarougui, S. & Elhallaoui, M. QSAR, molecular docking, ADMET properties in silico studies for a series of 7-propanamide benzoxaboroles as potent anti-cancer agents. *Chin. J. Anal. Chem.* **50**, 100163 (2022).
40. Golbraikh, A. & Tropsha, A. Beware of q2!. *J. Mol. Graph. Model.* **20**, 269–276 (2002).
41. Salt, D. W., Yildiz, N., Livingstone, D. J. & Tinsley, C. J. The use of artificial neural networks in QSAR. *Pestic. Sci.* **36**, 161–170 (1992).
42. Kůrková, V. Kolmogorov's theorem and multilayer neural networks. *Neural Netw.* **5**, 501–506 (1992).
43. Rücker, C., Rücker, G. & Meringer, M. y-Randomization and Its variants in QSPR/QSAR. *J. Chem. Inf. Model.* **47**, 2345–2357 (2007).
44. Tropsha, A., Gramatica, P. & Gombar, V. K. The importance of being earnest: validation is the absolute essential for successful application and interpretation of QSPR models. *QSAR Comb. Sci.* **22**, 69–77 (2003).
45. El fadili, M. et al. QSAR, ADME-Tox, molecular docking and molecular dynamics simulations of novel selective glycine transporter type 1 inhibitors with memory enhancing properties. *Heliyon* https://doi.org/10.1016/j.heliyon.2023.e13706 (2023).
46. Ed-Dahmani, I. et al. Phytochemical, antioxidant activity, and toxicity of wild medicinal plant of *Melitotus albus* extracts, in vitro and in silico approaches. *ACS Omega* https://doi.org/10.1021/acsomega.3c08314 (2024).
47. Nouioura, G. et al. *Petroselinum crispum* L. essential oil as promising source of bioactive compounds, antioxidant, antimicrobial activities: In vitro and in silico predictions. *Heliyon* **10**, e29520 (2024).
48. Abechi, S. E. et al. Virtual screening and pharmacokinetics analysis of inhibitors against tuberculosis: Structure and ligand-based approach. *Sci. Afr.* **23**, e02085 (2024).
49. Assaggaf, H. et al. GC/MS profiling, in vitro antidiabetic efficacy of origanum compactum benth. Essential oil and in silico molecular docking of its major bioactive compounds. *Catalysts* **13**, 1429 (2023).

50. Benkhaira, N. et al. Unveiling the phytochemical profile, in vitro bioactivities evaluation, in silico molecular docking and ADMET study of essential oil from *Clinopodium nepeta* grown in Middle Atlas of Morocco. *Biocatal. Agric. Biotechnol.* https://doi.org/10.1016/j.bcab.2023.102923 (2023).
51. El fadili, M. et al. In-silico investigations of novel tacrine derivatives potency against Alzheimer's disease. *Sci. Afr.* https://doi.org/10.1016/j.sciaf.2023.e02048 (2023).
52. Scalable algorithms for molecular dynamics simulations on commodity clusters. In *Proceedings of the 2006 ACM/IEEE Conference on Supercomputing.* https://doi.org/10.1145/1188455.1188544
53. Bowers, K. J. et al. Scalable algorithms for molecular dynamics simulations on commodity clusters. In *Proceedings of the 2006 ACM/IEEE Conference on Supercomputing* 84-es (Association for Computing Machinery, 2006). https://doi.org/10.1145/1188455.1188544.
54. Kumar, V. et al. 3D-QSAR-based pharmacophore modeling, virtual screening, and molecular dynamics simulations for the identification of spleen tyrosine kinase inhibitors. *Front. Cell. Infect. Microbiol.* **12**, 909111 (2022).
55. Li, Q. et al. Molecular dynamics simulation of the inhibition mechanism of factor XIa by Milvexian-like macrocyclic inhibitors. *Comput. Theor. Chem.* **1225**, 114131 (2023).
56. IJMS | Free Full-Text | Multifaceted Role of Matrix Metalloproteinases in Neurodegenerative Diseases: Pathophysiological and Therapeutic Perspectives. https://www.mdpi.com/1422-0067/22/3/1413
57. Uddin, Md. S. et al. Multifarious roles of mTOR signaling in cognitive aging and cerebrovascular dysfunction of Alzheimer's disease. *IUBMB Life* **72**, 1843–1855 (2020).
58. Mujwar, S. & Tripathi, A. Repurposing benzbromarone as antifolate to develop novel antifungal therapy for Candida albicans. *J. Mol. Model.* **28**, 193 (2022).
59. Shah, K., Mujwar, S., Krishna, G. & Gupta, J. K. Computational design and biological depiction of novel naproxen derivative. *ASSAY Drug Dev. Technol.* **18**, 308–317 (2020).
60. Er-Rajy, M., ElFadili, M., Mujwar, S., Zarougui, S. & Elhallaoui, M. Design of novel anti-cancer drugs targeting TRKs inhibitors based 3D QSAR, molecular docking and molecular dynamics simulation. *J. Biomol. Struct. Dyn.* **41**, 21. https://doi.org/10.1080/07391102.2023.2170471 (2023).
61. Molecules | Free Full-Text | Computational Bioprospecting Guggulsterone against ADP Ribose Phosphatase of SARS-CoV-2. https://www.mdpi.com/1420-3049/27/23/8287
62. Er-rajy, M. et al. QSAR, molecular docking, and molecular dynamics simulation-based design of novel anti-cancer drugs targeting thioredoxin reductase enzyme. *Struct. Chem.* **34**, 1527–1543 (2023).
63. Pharmaceutics | Free Full-Text | Indene-Derived Hydrazides Targeting Acetylcholinesterase Enzyme in Alzheimer's: Design, Synthesis, and Biological Evaluation. https://www.mdpi.com/1999-4923/15/1/94
64. Shinu, P. et al. Computational design, synthesis, and pharmacological evaluation of naproxen-guaiacol chimera for gastro-sparing anti-inflammatory response by selective COX2 inhibition. *Molecules* **27**, 6905 (2022).
65. Vickers, N. J. Animal communication: When I'm calling you, will you answer too?. *Curr. Biol.* **27**, R713–R715 (2017).
66. Hansch, C., Leo, A., Mekapati, S. B. & Kurup, A. QSAR and ADME. *Bioorg. Med. Chem.* **12**, 3391–3400 (2004).
67. Jin, Z. et al. Structure-based virtual screening of influenza virus RNA polymerase inhibitors from natural compounds: Molecular dynamics simulation and MM-GBSA calculation. *Comput. Biol. Chem.* **85**, 107241 (2020).
68. Golbraikh, A. et al. Rational selection of training and test sets for the development of validated QSAR models. *J. Comput. Aided Mol. Des.* **17**, 241–253 (2003).
69. El fadili, M. et al. An in-silico investigation based on molecular simulations of novel and potential brain-penetrant GluN2B NMDA receptor antagonists as anti-stroke therapeutic agents. *J. Biomol. Struct. Dyn.* **0**, 1–15 (2023).
70. El fadili, M. et al. 3D-QSAR, ADME-tox in silico prediction and molecular docking studies for modeling the analgesic activity against neuropathic pain of novel NR2B-selective NMDA receptor antagonists. *Processes* **10**, 1462 (2022).
71. Mao, F. et al. Melting point distribution analysis of globally approved and discontinued drugs: A research for improving the chance of success of drug design and discovery. *ChemistryOpen* **5**, 357–368 (2016).
72. Pires, D. E. V., Blundell, T. L. & Ascher, D. B. pkCSM: Predicting small-molecule pharmacokinetic and toxicity properties using graph-based signatures. *J. Med. Chem.* **58**, 4066–4072 (2015).
73. Ahmed, T. A. *Basic Pharmacokinetic Concepts and Some Clinical Applications* (BoD—Books on Demand, 2015).
74. Šrejber, M. et al. Membrane-attached mammalian cytochromes P450: An overview of the membrane's effects on structure, drug binding, and interactions with redox partners. *J. Inorg. Biochem.* **183**, 117–136 (2018).
75. Chandrasekaran, B., Abed, S. N., Al-Attraqchi, O., Kuche, K. & Tekade, R. K. Chapter 21—Computer-aided prediction of pharmacokinetic (ADMET) properties. In *Dosage Form Design Parameters* (ed. Tekade, R. K.) 731–755 (Academic Press, 2018). https://doi.org/10.1016/B978-0-12-814421-3.00021-X

Acknowledgements

Author contributions

M.A: Writing—original draft, Methodology, Investigation, Data curation, Conceptualization. M.E–f: Investigation, Formal analysis, Conceptualization. SM: Supervision, Software, Resources. M.E-r: Methodology, Investigation, Conceptualization. H.A.A: Data curation, Resources, Project administration. S.E-r: Writing—review & editing, Resources. S.Z: Writing—original draft, Formal analysis. M.E: Visualization, Supervision.

Funding

Declarations

Competing interests

The authors declare no competing interests.

Additional information

Supplementary Information The online version contains supplementary material available at https://doi.org/10.1038/s41598-025-98182-x.

Correspondence and requests for materials should be addressed to M.A. or M.E.f.

Reprints and permissions information is available at www.nature.com/reprints.

Publisher's note Springer Nature remains neutral with regard to jurisdictional claims in published maps and institutional affiliations.